Yheskel *et al. Epigenetics & Chromatin* (2025) 18:78
https://doi.org/10.1186/s13072-025-00644-z

Epigenetics & Chromatin

RESEARCH Open Access

Local chromatin context informs transcriptional outcomes for the histone demethylase KDM5

Matanel Yheskel[1], Melissa A. Castiglione[1] and Julie Secombe[1,2*]

Abstract

Background Lysine demethylase 5 (KDM5) family proteins are transcriptional regulators best known for demethylating the promoter-proximal histone mark H3K4me3. KDM5-mediated regulation of gene expression is crucial in the brain, with pathogenic variants in human *KDM5* genes leading to intellectual disability (ID) disorders. Although the demethylase activity of KDM5 proteins is vital for brain function, non-enzymatic functions also contribute. How KDM5 uses distinct features to regulate transcription in a context-dependent manner remains largely uncharacterized.

Results Using *Drosophila*, we demonstrate that a demethylase-dead $Kdm5^{JmjC*}$ strain expands the distribution of promoter-proximal H3K4me3 in the brain, whereas $Kdm5^{L854F}$, which models a pathogenic ID variant, has limited effects. Despite these divergent enzymatic effects, $Kdm5^{L854F}$ and $Kdm5^{JmjC*}$ exhibit similar transcriptional changes that do not correlate with changes to promoter recruitment of variant proteins, H3K4me3 levels, or chromatin accessibility. Instead, altered gene expression in both alleles correlates with preexisting chromatin signatures.

Conclusions These findings suggest that KDM5 operates in conjunction with local chromatin contexts to employ demethylase-dependent and independent mechanisms of gene expression regulation in the brain. Disruption to this regulation affects pathways critical for neuronal function and is likely to contribute to the cognitive and behavioral features seen in patients.

Keywords KDM5, Histone demethylase, Transcription, Chromatin, Brain, Intellectual disability, Claes-Jensen syndrome, KDM5C-NDD

*Correspondence:
Julie Secombe
julie.secombe@einsteinmed.edu
[1]Department of Genetics, Albert Einstein College of Medicine, Bronx, NY 10461, USA
[2]Dominick P. Purpura Department of Neuroscience, Albert Einstein College of Medicine, Bronx, NY 10461, USA

Background

The KDM5 family of enzymes are multidomain transcriptional regulators with roles across a wide range of cell types. Their activity is especially important in the nervous system, where they are required for proper brain development and function. This is based on the observation that genetic disruption to three of the four human *KDM5* paralogs, *KDM5A*, *KDM5B*, and *KDM5C*, is observed in individuals with neurodevelopmental disorders characterized by intellectual disability (ID), seizures, and changes in behavior and movement [1–4]. Critical roles for KDM5 proteins in the nervous system are evolutionarily conserved, as evidenced by the altered learning and memory, social interactions, aggression, and seizure susceptibility observed in animals with genetic knockout of *Kdm5a*, *Kdm5b*, or *Kdm5c* in *Mus musculus* [5–8]. In invertebrates such as *Drosophila melanogaster*, disruption to the function of their single *Kdm5* gene leads to cognitive, neuronal, and behavioral phenotypes consistent with those observed in humans [9–11].

Of the *KDM5* paralogs implicated in human ID disorders, *KDM5C* has been studied the most extensively. Pathogenic variants in *KDM5C* cause a neurodevelopmental disorder known as KDM5C-related neurodevelopmental disorder (KDM5C-NDD; also known as Claes-Jensen X-linked Intellectual disability syndrome), which consistently and dramatically affects hemizygous males [1, 7, 12, 13]. Approximately half of the known KDM5C-NDD variants are nonsense, frameshift, or other changes expected to lead to loss or reduced levels of KDM5C protein [1, 13]. The remainder are missense variants, which provide a powerful means to garner insights into the etiology of KDM5C-NDD and to dissect the molecular mechanisms by which KDM5 family proteins regulate transcription. ID-associated single amino acid changes occur throughout the KDM5C protein, including in the Jumonji C (JmjC) domain, which functions in conjunction with JmjN to form the enzymatic active site of KDM5 proteins [1, 3]. The combined activity of the JmjN/C domains demethylates trimethylated lysine 4 of histone H3 (H3K4me3), a promoter-proximal histone modification associated with transcriptional activation and consistency [14–16]. In keeping with a key neuronal role for this demethylase activity, some cognitive and behavioral phenotypes of *Kdm5c* knockout mice can be partially suppressed by genetically restoring levels of H3K4me3 [17]. In addition, a JmjC domain mutant *Drosophila* strain that lacks demethylase activity ($Kdm5^{JmjC^*}$) displays altered learning and memory, seizure susceptibility, locomotion, and neurotransmission [9, 11].

Despite the clear contribution of KDM5C's enzymatic activity to proper brain development, its loss alone is insufficient to explain the pathogenesis of KDM5C-NDD. Indeed, many missense variants occur outside of the enzymatic JmjN/JmjC domains, and several of these retain some in vitro demethylase activity [1, 13]. These data suggest that demethylase-dependent and independent effects on gene expression contribute to the traits observed. This is consistent with a broader body of literature on KDM5 proteins, which suggests that they possess demethylase-independent gene regulatory functions [1, 2, 18–20]. When and where these non-canonical KDM5 activities are utilized in vivo, their relationship to the histone demethylase activity, and whether KDM5 proteins can also impact gene regulation through additional activities, remains unclear. Analyses of ID-associated alleles offer an opportunity to uncover new gene-regulatory activities of KDM5 proteins and to provide insights into the links between KDM5 and neuronal (dys)function.

Here, we use *Drosophila* to investigate KDM5 function using an allele associated with severe intellectual disability, ataxia, and aggression ($KDM5C^{L731F}$) [21, 22]. This variant occurs within the C5HC2 zinc finger immediately adjacent to the JmjC domain, and a recombinant form of this protein displays a 2-fold decrease in in vitro enzymatic activity [23]. To understand the properties of this variant protein in an in vivo context, we generated a fly model of this allele in which *Drosophila Kdm5* encodes the equivalent of $KDM5C^{L731F}$ ($Kdm5^{L854F}$) as part of a library of human ID-associated allele variant strains for which we carried out transcriptomic and behavioral studies [9–11]. Both the demethylase-dead $Kdm5^{JmjC^*}$ and $Kdm5^{L854F}$ adult flies exhibit deficits in associative memory and altered locomotion [9, 10]. However, while western blot studies show that $Kdm5^{JmjC^*}$ causes a 2-fold increase in bulk levels of H3K4me3, $Kdm5^{L854F}$ does not, suggesting that the $KDM5^{L854F}$ variant protein retains at least some of its enzymatic activity in vivo [9, 10]. Here, we demonstrate that the changes in gene expression observed in the adult brains of $Kdm5^{JmjC^*}$ and $Kdm5^{L854F}$ animals cannot be explained by alterations in H3K4me3. Instead, we find that preexisting chromatin marks, including high levels of H3K4me3, promoter accessibility, and other chromatin features, correlate with the altered gene expression patterns seen in $Kdm5^{JmjC^*}$ and/or $Kdm5^{L854F}$. This suggests that the JmjC and/or the C5HC2 domains of KDM5 work in concert with existing histone modification landscapes to activate or repress transcription. These distinct modes of gene regulation by KDM5 are necessary to regulate pathways critical to various aspects of neuronal development and function, providing possible etiological links to the cognitive features observed in patients.

Methods

Fly strains and care

Fly food (per liter) contained 80 g malt extract, 65 g cornmeal, 22 g molasses, 18 g yeast, 9 g agar, 2.3 g methyl

para-benzoic acid, and 6.35 mL propionic acid per liter. Flies were kept at 25 °C with a 12-hour light/dark cycle and 50% humidity. All flies were collected or harvested 1–5 days after eclosion from 9:00 a.m. to 12:00 p.m. *Kdm5*$^{\Delta}$ (null allele; previously *Kdm5*^{140}), *Kdm5*^{JmjC*}, and *Kdm5*^{L854F} are published [9, 24, 25]. UAS-Dam:*Kdm5*-ID variant constructs were generated by site-directed mutagenesis of published UAS-Dam:*Kdm5* [25]. UAS-Dam was obtained from Dr. Andrea Brand's lab. All Dam fusion transgenes were inserted into attP2 on chromosome III. All transgenesis was carried out at Best Gene. The Ubi-Gal4 (RRID: BDSC_32551) fly stock was obtained from Bloomington *Drosophila* Stock Center.

Structural modeling

Protein structure predictions were performed using AlphaFold 3, hosted by DeepMind, using default parameters. Full-length FASTA files containing the amino acid sequences for *Drosophila* KDM5^{WT}, KDM5^{JmjC*}, and KDM5^{L854F} and their KDM5C equivalents were used as inputs in separate runs of the AlphaFold pipeline, and the predicted structures produced were later visualized, annotated, and aligned using ChimeraX [26, 27]. Per-residue root-mean-square deviation (RMSD) values were calculated to assess structural differences between AlphaFold-generated protein data banks (PDBs) of either KDM5^{WT} and KDM5^{JmjC*} or KDM5^{L854F} proteins. Structures were loaded using the MDAnalysis Python library and aligned using a least-squares fit based on alpha carbon (Cα) atoms. Residue numbers were matched between structures to ensure one-to-one comparison.

Targeted DamID (TaDa)

Tissue processing was performed as previously described with the following modifications: TaDa was performed in triplicate (*Kdm5*^{L854F} in duplicate) for each genotype with 10 heads per sample [25]. KDM5-DamID fusion proteins were expressed under the control of Ubi-Gal4, which was pulsed on for three days during early adulthood. Genotypes were *Kdm5*$^{\Delta}$, Ubi-Gal4/*Kdm5*$^{\Delta}$, tubulin-Gal80^{ts}; UAS-*Kdm5:DamID*$^{WT\ or\ variant}$, *gKdm5:HA*$^{WT\ or\ variant}$. Samples were homogenized in 75µL UltraPure Distilled Water and 20µL 500mM EDTA, then digested with Proteinase K for 1.5 h. DNA extraction was performed using the Zymo Quick-DNA Miniprep Plus Kit (Zymo, D3024). DpnI digestion, PCR adaptor ligation, DpnII digestion, and PCR amplification were performed as described. DNA was sonicated using a Diagenode Bioruptor Pico for six cycles (30 s on/90 seconds off at 4 °C), and the resulting DNA fragments were analyzed using an Agilent Bioanalyzer to confirm ~ 300 bp fragment size. DamID adaptor removal and DNA cleanup were performed as previously described. The samples were then submitted to BGI Genomics for library construction and sequencing. Libraries were prepared at BGI Genomics following a ChIP-seq workflow and sequenced on the NovaSeq S4.

For TaDa analyses, sequencing data were aligned to the *D. melanogaster* dm6 genome and processed using damidseq_pipeline [28]. After converting to bedgraphs via damidseq_pipeline, peaks were called using find_peaks (using the parameters fdr = 0.05, min_quant = 0.8) on the averaged replicates, and genes overlapping peaks were identified using ChIPSeeker [29]. We used NOISeq to perform differential analysis comparing KDM5^{JmjC*} and KDM5^{L854F} to KDM5^{WT}, using a standard cutoff of 0.8 for statistical significance [30, 31].

Single-cell suspension

50 brains were dissected and placed in 1 mL of ice-cold 1X PBS. Brains were centrifuged at 4 °C for 5 min at 1000XG. PBS was removed and the cell pellet was resuspended with 150 µL of 100 mg/mL Collagenase, Type I (ThermoFisher, 17018029) and incubated at 25 °C on a thermoshaker at 500 rpm for 2 h. The suspension was vigorously pipetted up and down 20 times every 10–15 min to facilitate digestion. After incubation, suspensions were centrifuged again at 4 °C for 5 min at 1000XG and resuspended in PBS + 10% DMSO. 10 µL of the suspension was used for cell quantification using a hemocytometer. 50 brains yielded about 1.5 million cells. The remaining 100 µL was slowly frozen using a Mr. Frosty Freezing Container (ThermoFisher, 5100-0001) at -80 °C.

CUT & RUN

CUT & RUN was performed using the Epicypher CUTANA Kit (Epicypher, 14-1048) and Epicypher Library Prep Kit (Epicypher, 14-1001), as directed, with the generated single-cell suspension. The anti-H3K4me3 antibody used was Epicypher Cat# 13–0041 (RRID: AB_3076423), and IgG (Epicypher Cat# 13–0042, RRID: AB_2923178). Samples were sequenced on the Illumina MiSeq Platform. All samples were normalized to spike-in *E. coli* DNA.

ATAC-Seq

ATAC-Seq was performed using the ATAC-Seq Kit from Active Motif (Active Motif, 53150) using adult brains following the manufacturer's instructions. Samples were sequenced on the Illumina MiSeq Platform.

Peak alignment and analysis

Raw reads were quality controlled and trimmed using rfastp (v1.6.0) and were aligned using Rsubread (2.10.5) to the dm6 *Drosophila melanogaster* genome assembly [32, 33]. BAM files were normalized by dividing the number of *E.coli* reads in each sample by the lowest number of *E. coli* reads across samples. Samtools (v1.14) was

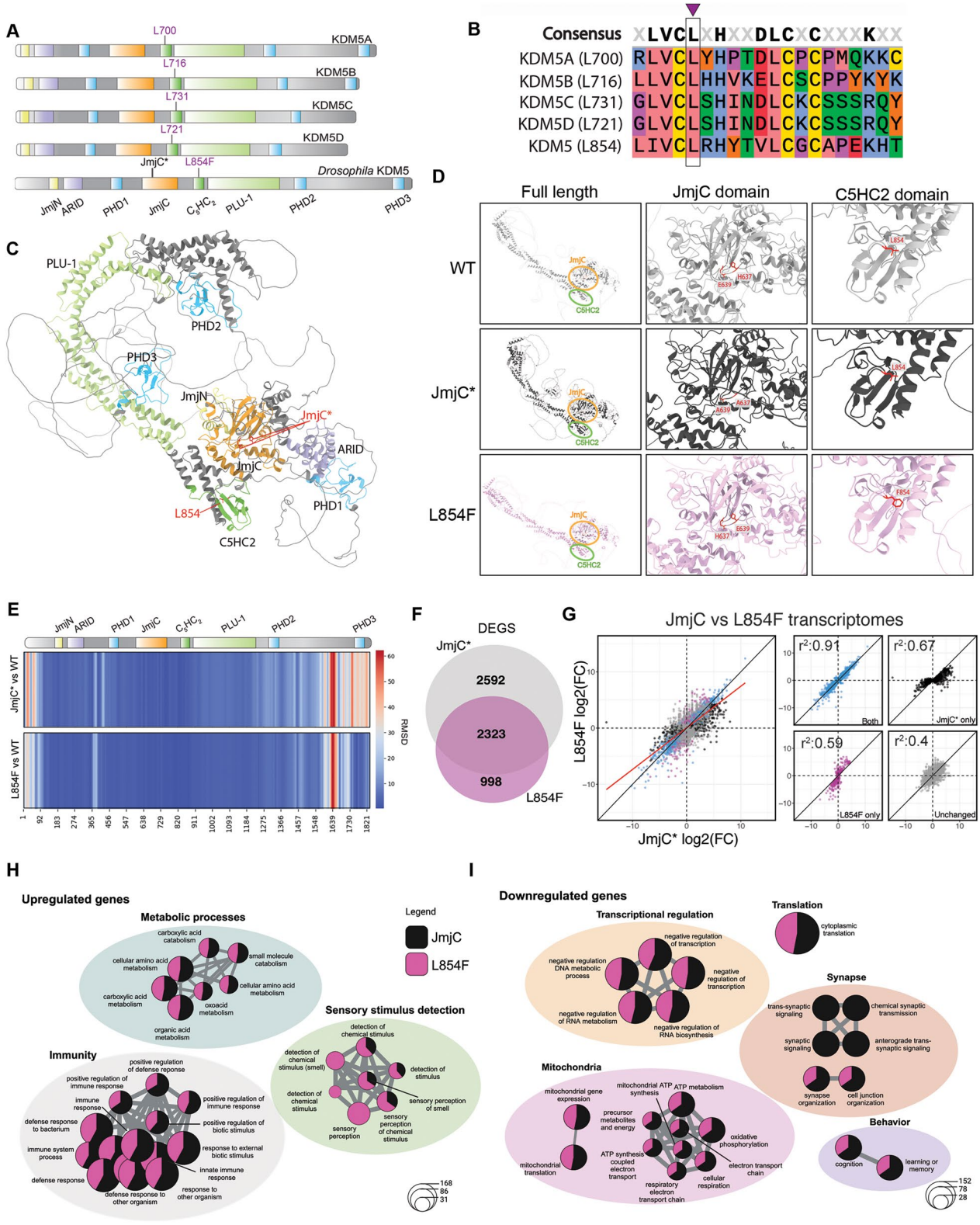

Fig. 1 (See legend on next page.)

(See figure on previous page.)

Fig. 1 KDM5^{JmjC*} and KDM5^{L854F} are structurally alike and have similar overall changes to gene expression. **A** Schematic of the ID-associated KDM5C^{L731F} variant and the analogous residue in human KDM5A, KDM5B, KDM5D, and *Drosophila* KDM5. *Kdm5^{JmjC*}* in *Drosophila* is a demethylase-dead strain. **B** Alignment of human KDM5A, KDM5B, KDM5C, KDM5D, and *Drosophila* KDM5 showing amino acid conservation. Leucine 731 of KDM5C is conserved across all KDM5 proteins shown (box and arrowhead). **C** AlphaFold model of *Drosophila* KDM5 visualized using ChimeraX. Domains are indicated using the same color as in **A**, and bubbles show residues considered in this study. In black are the two residues which bind to the iron molecule necessary for demethylation (H637A and E639A; altered in KDM5^{JmjC*}) and in purple is the L854F change that occurs within the C5HC2 zinc finger. **D** AlphaFold models of *Drosophila* KDM5^{WT}, KDM5^{JmjC*}, and KDM5^{L854F} proteins, with C5HC2 and JmjC domains highlighted. The first column shows full-length proteins. The second column shows the JmjC domain in KDM5^{WT}, KDM5^{JmjC*}, and KDM5^{L854F} proteins. The side chains altered in the demethylase-dead KDM5^{JmjC*} protein (positions 637 and 6390), are highlighted in red. The third column shows the C5HC2 domain in KDM5^{WT}, KDM5^{JmjC*}, and KDM5^{L854F} proteins. The side chain at 854 is shown in red. **E** Predicted structural differences between AlphaFold-generated PDBs of KDM5^{WT} and KDM5^{JmjC*} (top) or KDM5^{L854F} (bottom) proteins using per-residue root-mean-square deviation (RMSD) values. The N and C termini are intrinsically disordered, making them difficult to predict via AlphaFold, which results in a greater RMSD between the modeled structures. **F** Venn diagram showing the overlap in differentially expressed genes (DEGs) in *Kdm5^{JmjC*}* and *Kdm5^{L854F}* RNA-seq from adult heads using 5% false discovery rate (FDR) cutoff for significance. **G** Scatterplots of RNA-Seq log2(FC)s from *Kdm5^{L854F}* and *Kdm5^{JmjC*}*. Blue = DEG in both genotypes, black = DEG in *Kdm5^{JmjC*}* only, purple = DEG in *Kdm5^{L854F}* only, and gray = unchanged in both. **H** GO analysis of genes upregulated in *Kdm5^{JmjC*}* and/or *Kdm5^{L854F}* using clusterProfiler, in which the size of each circle corresponds to the number of genes in the GO category, and the size of each pie slice corresponds to the relative number of genes in each category attributed to that genotype, according to color. **I** GO analysis of downregulated genes using clusterProfiler, using similar notation to **H**

then used to scale BAM files by this normalization factor using (samtools view -s (normalization factor)) [34]. BigWigs were generated using the deepTools (v3.5.1) bamCoverage function [35]. Profiles and heatmaps were generated using the deepTools computeMatrix and plotProfile functions. Peaks were called using Genrich(v0.6.1) and DiffBind (v3.6.1) was used to perform differential peak analyses [36, 37]. Reads in each peak were counted using dba.count(summits = FALSE). ChIPSeeker (v1.32.0) was used to perform peak annotation, and clusterProfiler(v4.4.4) was used to perform Gene Ontology Analyses [29, 38].

Signal quantification and plotting

ChIP-seq and CUT&RUN data at specific genomic regions were plotted using PyGenomeTracks (v3.8) [39, 40]. Graphs were generated using ggplot2 [41]. Mean signal intensities were calculated from promoter-proximal regions TSS ± 100 bp and gene body regions (TSS + 300 bp to + 800 bp) using BED files defining these intervals in combination with the *MultiBigwigSummary* tool in deepTools (v 3.5.1) [35]. Signal quantification data for all of the chromatin marks examined are provided in Table S2.

Published datasets used in the study

Kdm5^{JmjC*} and *Kdm5^{L854F}* RNA-seq data derived from adult heads have been previously published and are available at GEO: GSE100578 and GEO: GSE245380 [9, 11]. KDM5 ChIP-seq from whole adult flies is published and publicly available (GSE70589) [42]. The following ChIP-seq datasets were generated as part of the ModEncode project using heads from *Oregon R* adults: H3K36me3 (SRX287816; GEO accession GSM1147324), H3K9ac(SRX287708; GEO accession GSM1147220), H2Bub (SRX287772; GEO accession GSM1147284), H4K20me1 (SRX287663; GEO accession GSM1147175), RNA Polymerase II (Polr2A; SRX287911; GEO accession GSM1147419) [43]. All datasets were mapped to *dm6* and were downloaded from the ChIP-ATLAS database [44].

Results

Kdm5^{L854F} and *Kdm5^{JmjC*}* show unique and overlapping changes to gene expression

The ID-associated variant KDM5^{L854F} (equivalent to KDM5C^{L731F}) occurs within the C5HC2 zinc finger domain and consistent with its functional importance, it is conserved in human KDM5A, KDM5B, KDM5C, and KDM5D (Fig. 1A, B). To understand the defects caused by this variant, we compared it to the demethylase-dead *Kdm5^{JmjC*}* strain, which encodes a form of KDM5 with changes to the active site of the JmjC domain that abolish its enzymatic activity (H637A and E639A; Fig. 1C) [9–11, 45, 46]. In silico modeling of *Drosophila* KDM5^{JmjC*} and KDM5^{L854F} and their human KDM5C equivalents using AlphaFold revealed that the amino acid substitutions did not grossly alter their predicted structure (Fig. 1D; Figure S1A, B) [26]. Moreover, the leucine at position 731/854 is not expected to interact with structural components of the protein that are necessary to maintain the enzymatic demethylation pocket (Fig. 1D; Fig. S1A). Per-residue root mean square deviation (RMSD) values comparing the predicted structures of *Drosophila* KDM5^{WT} and KDM5^{JmjC*} or KDM5^{L854F} were low, indicating that they are similar, apart from the disordered regions at the N and C termini that are inherently difficult to model (Fig. 1E). Furthermore, the introduction of a bulky phenylalanine in the variant KDM5^{L854F} protein is not predicted to affect the structure of the C5HC2 motif, or the neighboring JmjC domain. Neither KDM5^{JmjC*} nor KDM5^{L854F} is likely to dramatically disrupt the overall folding of the protein [9, 10].

To directly compare the transcriptional effects of *Kdm5^{JmjC*}* and *Kdm5^{L854F}*, we utilized previously generated RNA-seq data from adult heads. These datasets were collected as part of a broader study of five ID-variant fly

strains that centered on their shared impact on translation-related gene expression [9, 11]. Comparing the gene expression changes observed in *Kdm5*^{L854F} and *Kdm5*^{JmjC*}, we find that many of the significantly dysregulated genes in both genotypes exhibit similar behavior (r^2 = 0.91; p = 2.2e-16; Fig. 1F, G; Table S1). Consistent with this, *Kdm5*^{L854F} and *Kdm5*^{JmjC*} shared many Gene Ontology (GO) categories, including metabolism and immunity among the upregulated genes, and translation and mitochondrial function among the downregulated genes (Fig. 1H, I). There were also GO categories that were unique to one genotype or the other. For example, *Kdm5*^{JmjC*} showed a greater enrichment for gene categories involving synaptic signaling, while *Kdm5*^{L854F} had more genes involved in sensory perception.

To determine which genes dysregulated in *Kdm5*^{JmjC*} and K*dm5*^{L854F} were likely to be directly regulated by KDM5, we integrated transcriptomic information with ChIP-seq data derived from whole adult flies.[42] 58% and 56% of dysregulated genes had an associated KDM5 promoter peak for *Kdm5*^{JmjC*} and *Kdm5*^{L854F}, respectively (Fig. 2A, B; Table S1). These included similar numbers of up- and downregulated genes, consistent with studies implicating KDM5 proteins as both repressors and activators of gene expression (Fig. 2C, D).[18,46] Interestingly, directly regulated genes generally showed smaller changes in gene expression than indirect targets (Fig. 2C-G). To explore potential underlying reasons for this, we compared the expression of KDM5-bound and non-bound genes based on average normalized expression counts and RNA polymerase II (Pol II) occupancy using adult head ChIP-seq data from the modENCODE project [43, 44, 47]. KDM5-bound genes showed significantly higher expression and gene body Pol II levels than non-bound genes, which likely contributed to the lower fold change observed at direct target genes (Fig. 2H; Fig. S2A; Table S2). The higher level of gene expression was observed across KDM5-bound genes that were upregulated, downregulated, or unchanged in both *Kdm5*^{JmjC*} and *Kdm5*^{L854F} (Fig. S2B-E). KDM5 therefore binds to and modulates the expression of genes that are robustly expressed. Genes that were directly regulated in both *Kdm5*^{JmjC*} and *Kdm5*^{L854F} mutants were enriched for shared GO categories. Among downregulated genes, mitochondrial and translation-related processes were prominent, while upregulated genes were enriched for immune-related functions (Fig. 2I). Further emphasizing the concordance of the *Kdm5*^{JmjC*} and *Kdm5*^{L854F} datasets, 97% of the direct targets that were dysregulated in both genotypes behaved similarly (r^2 = 0.9; Fig. 2J). In addition to possessing unique functions, the adjacent JmjC and C5HC2 domains of KDM5 are therefore jointly required to increase or dampen the expression of many genes.

KDM5^{JmjC*} but not KDM5^{L854F} broadly expands promoter-proximal H3K4me3 peaks

Our prior western blot studies of adult heads showed that while *Kdm5*^{JmjC*} animals show a 2-fold increase in levels of H3K4me3, levels of this chromatin mark in *Kdm5*^{L854F} were similar to wild type [9]. To accurately assess the effects of the variant KDM5^{L854F} protein on H3K4me3 levels across the genome in the adult brain, and compare these to those of KDM5, we used *C*leavage *U*nder *T*argets & *R*elease *U*sing *N*uclease (CUT&RUN) [48, 49]. In *Kdm5*^{WT} animals, H3K4me3 was observed surrounding the transcriptional start sites (TSSs) and coincided with regions bound by KDM5 (Fig. 3A, Fig. S3A, B) [42, 50]. Since H3K4me3 is typically enriched at active genes, this aligns with our observation that KDM5 preferentially binds to highly expressed genes. (Fig. 2H; Fig. S2A-E). H3K4me3 was expanded at KDM5-bound promoters in *Kdm5*^{JmjC*} animals, as anticipated (Fig. 3A-C). Quantification of the differences in H3K4me3 in *Kdm5*^{JmjC*} brains compared to *Kdm5*^{WT} using Diffbind identified 1516 KDM5-bound genes with significantly increased signal intensity and four genes with reduced signal (log2FC > ± 1 and FDR < 0.01 cutoffs; Fig. 3D; Table S3) [51]. Changes to H3K4me3 did not, however, predict transcriptional outcomes. Of the 1516 genes with increased H3K4me3, 41% showed decreased gene expression, 34% increased, and 25% remained unchanged or were expressed at very low levels (Fig. 3E). We also used Diffbind data to examine how the extent of H3K4me3 increase (ΔH3K4me3) related to transcriptional changes across the genome and at genes with significantly increased H3K4me3. Overall, this revealed that genes that were upregulated or unchanged showed similarly increased H3K4me3, while downregulated genes exhibited a slightly greater change to H3K4me3 (Fig. S3C, D). These findings indicate that while KDM5 broadly regulates promoter H3K4me3, changes to this mark alone are insufficient to explain the transcriptional outcomes of *Kdm5*^{JmjC*} animals.

In contrast to *Kdm5*^{JmjC*}, the overall profile of H3K4me3 in *Kdm5*^{L854F} was similar to *Kdm5*^{WT} (Fig. 3A-C; Fig. S3A, B). Diffbind detected 195 genes with increased H3K4me3 in *Kdm5*^{L854F} animals, 98% of which overlapped and were well correlated with those that were observed in *Kdm5*^{JmjC*} (191 genes; $r^2 = 0.36$ $p < 0.001$; Fig. 3F-H; Table S3). Examining the 191 genes that showed increased H3K4me3 in *Kdm5*^{JmjC*} and *Kdm5*^{L854F}, we observe that a majority show no change to gene expression or were not expressed in either *Kdm5*^{JmjC*} or *Kdm5*^{L854F} (135 genes; 71%; three genes were not detectably expressed; Fig. 3I). Of the 56 genes that were dysregulated, 34% were upregulated and 41% were downregulated (Fig. 3I). Although no link with altered expression was observed, we do note that all 188 genes with increased H3K4me3 were highly

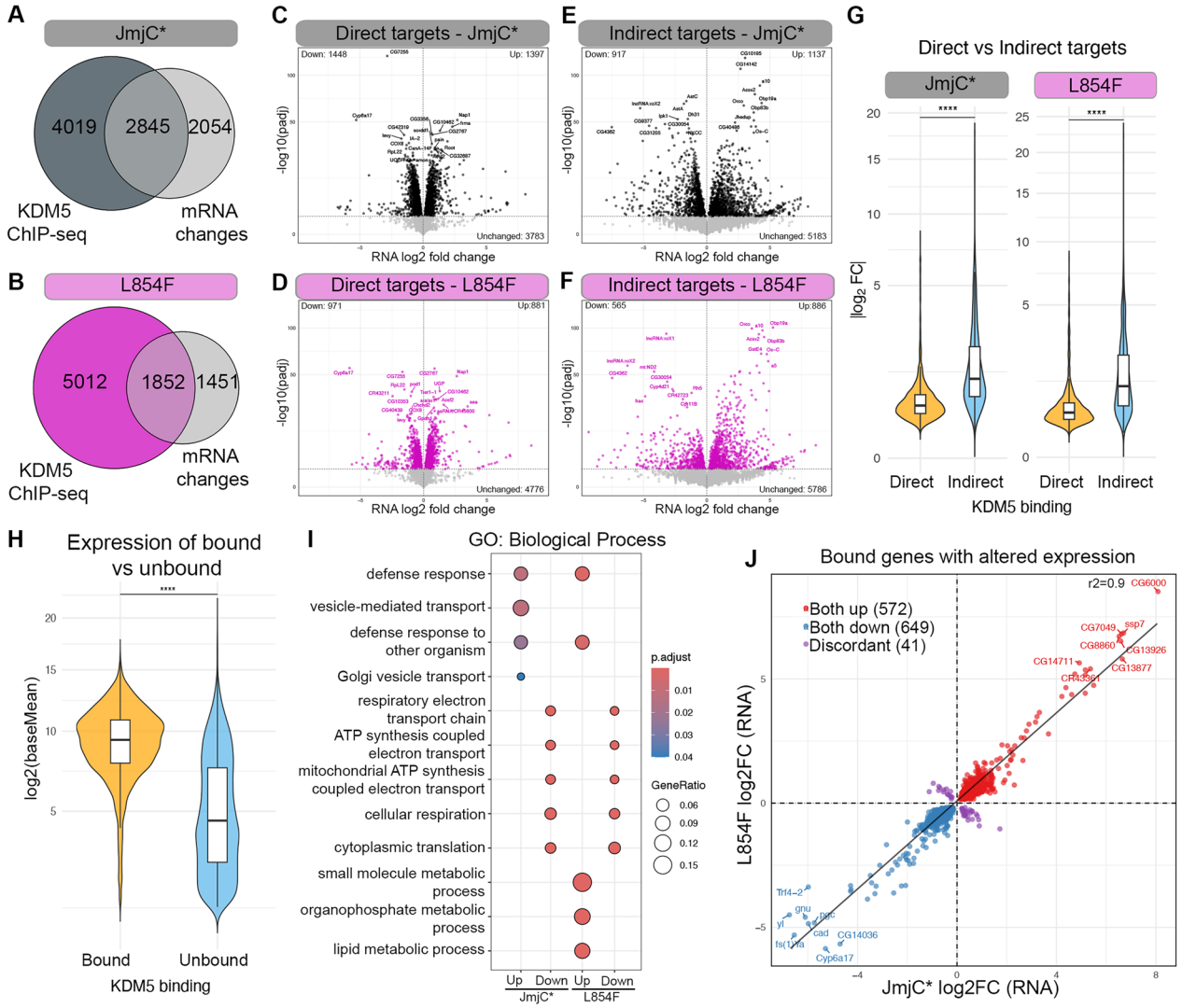

Fig. 2 Direct and indirect changes to gene expression in *Kdm5*^{JmjC*} and *Kdm5*^{L854F}. **A** Venn diagram showing overlap between genes bound by KDM5 based on ChIP-seq data from whole adult flies and changes to gene expression in *Kdm5*^{JmjC*} (both up- and downregulated genes; 58% of differentially expressed genes (DEGs)). **B** Venn diagram showing overlap between genes bound by KDM5 and changes to gene expression in *Kdm5*^{L854F} (both up- and downregulated genes; 56%). **C** Volcano plot showing the distribution of directly regulated genes in *Kdm5*^{JmjC*}, using a 5%FDR for DEGs. Significantly affected genes are indicated by black dots. **D** Volcano plot showing the distribution of directly regulated genes in *Kdm5*^{L854F}, using a 5%FDR for DEGs. Significantly affected genes are indicated by purple dots. **E** Volcano plot showing distribution of indirectly regulated (no promoter-associated KDM5 binding) genes in *Kdm5*^{JmjC*}, using 5%FDR for DEGs. Significantly affected genes are indicated by black dots. **F** Volcano plot showing the distribution of indirectly regulated (no promoter-associated KDM5 binding) genes in *Kdm5*^{L854F}, using a 5%FDR for DEGs. Significantly affected genes are indicated by purple dots. **G** Absolute log2 fold change (combining up- and downregulated into |log2 fold change|) for directly (orange) and indirectly (light blue) regulated genes from *Kdm5*^{JmjC*} (left) and *Kdm5*^{L854F} (right). **** $p < 0.0001$). **H** Violin plots showing normalized expression count (baseMean) values at KDM5-bound (orange; 6519 genes) and unbound (blue; 6950 genes) genes. **** $p < 0.0001$ (Kruskal-Wallis test). **I** Gene ontology (biological process) analysis comparing directly up- and downregulated genes in *Kdm5*^{JmjC*} and *Kdm5*^{L854F}. **J** Scatterplot showing the similarity in gene expression changes of direct targets in *Kdm5*^{JmjC*} and *Kdm5*^{L854F}. The number of genes in each category is indicated in the top left

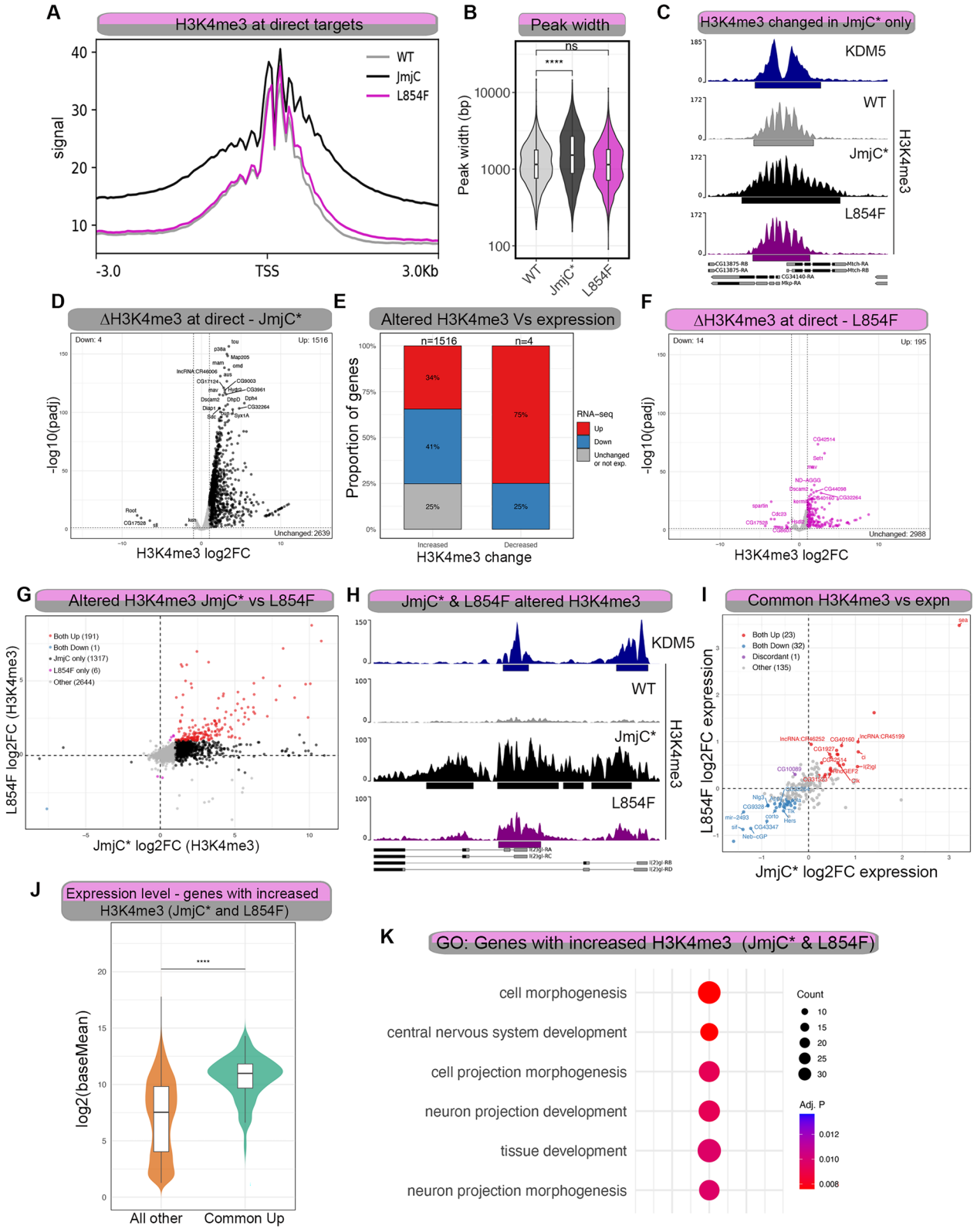

Fig. 3 (See legend on next page.)

(See figure on previous page.)

Fig. 3 Increased promoter H3K4me3 does not correlate with changes to mRNA levels. **A** Transcriptional start site (TSS) profiles of H3K4me3 CUT&RUN at KDM5-bound genes (direct targets) from $Kdm5^{WT}$ (grey), $Kdm5^{JmjC*}$ (black), $Kdm5^{L854F}$ (purple). **B** H3K4me3 peak widths from $Kdm5^{WT}$ (grey; median of 1152 bp), $Kdm5^{JmjC*}$ (black; median of 1524 bp), $Kdm5^{L854F}$ (purple; median of 1145). **** p-value < 0.0001 Kruskal-Wallis test. ns = not significant. **C** Genome track of CUT&RUN data from $Kdm5^{WT}$ (grey), $Kdm5^{JmjC*}$ (black), and $Kdm5^{L854F}$ (purple), showing a genomic region with KDM5 binding and increased H3K4me3 in $Kdm5^{JmjC*}$ but not $Kdm5^{L854F}$ [42]. Bars beneath each track show the called peaks from the associated BED file. **D** Volcano plot showing KDM5-bound genes with changes in H3K4me3 (Diffbind analysis) in $Kdm5^{JmjC*}$. Black dots indicate genes with altered H3K4me3 (log2FC ± 1 and FDR < 0.01). **E** Stacked bar graph separating genes with significantly increased (left) or decreased (right) H3K4me3 and the proportion of those genes that show altered gene expression based on RNA-seq data. $n = 1516$ and 4 genes for increased and decreased H3K4me3, respectively. **F** Volcano plot showing KDM5-bound genes with changes in H3K4me3 (Diffbind analysis) in $Kdm5^{L854F}$. Purple dots indicate genes with significantly changed H3K4me3 (log2FC ± 1 and FDR < 0.01). Note the same y-axis limits as **D**. **G** Scatterplot showing correlation between changes to H3K4me3 (using Diffbind) for direct target genes for $Kdm5^{JmjC*}$ (x-axis) and $Kdm5^{L854F}$ (y-axis). Red dots indicate genes with altered H3K4me3 in both, black shows $Kdm5^{JmjC*}$ only, purple dots indicate genes altered in $Kdm5^{L854F}$ only, and gray indicates other categories. Gene number for each category are indicated. **H** Genome track of H3K4me3 CUT & RUN data from $Kdm5^{WT}$ (grey), $Kdm5^{JmjC*}$ (black), $Kdm5^{L854F}$ (purple), showing increased H3K4me3 at *l(2)gl gene* in $Kdm5^{JmjC*}$ and $Kdm5^{L854F}$. Bars indicate called peaks from BED file. **I** Scatterplot showing only the 191 genes with significantly increased H3K4me3 in both $Kdm5^{JmjC*}$ and $Kdm5^{L854F}$, showing changes to gene expression in each genotype. The x-axis shows $Kdm5^{JmjC*}$ log2FC RNA-seq data, and the y-axis shows $Kdm5^{L854F}$ data. Most genes show unaltered gene expression (or no expression) in both genotypes (gray; 135 genes). Red dots indicate genes upregulated in both genotypes ($n = 23$); blue dots indicate downregulation in both genotypes ($n = 32$). **J** Violin plots showing baseMean signal from the 188 expressed genes with increased H3K4me3 in $Kdm5^{JmjC*}$ and $Kdm5^{L854F}$ (green) and other expressed genes (orange; $n = 13677$). **K** Gene ontology using the 188 highly expressed genes that showed increased H3K4me3 in $Kdm5^{JmjC*}$ and $Kdm5^{L854F}$

expressed based on examining expression and RNA polymerase II data (Fig. 3J; Fig. S3E-G). The high expression of these 188 genes, including Wiskott-Aldrich Syndrome Protein (WASp) and Neuroglian (Nrg) that are important for neuronal cytoskeletal organization and adhesion, may make them especially susceptible to H3K4me3 changes (Fig. 3K). Overall, we conclude that $KDM5^{L854F}$ retains sufficient enzymatic function to maintain H3K4me3 levels at most genes. This suggests that the underlying pathomechanism for this variant in intellectual disability is not simply the loss of enzymatic function.

Changes to promoter recruitment or accessibility do not account for the changes in H3K4me3 or gene expression observed in $Kdm5^{JmjC*}$ and $Kdm5^{L854F}$ animals

One possible contributor to the changes in H3K4me3 and/or gene expression caused by $KDM5^{JmjC*}$ and $KDM5^{L854F}$ variant proteins is altered recruitment. To test this, we performed *Ta*rgeted *Da*mID (TaDa) in adult brains, comparing the behavior of $KDM5^{JmjC*}$ and $KDM5^{L854F}$ with that of wild-type KDM5 [25, 52–54]. To ensure the appropriate genetic background, we induced the expression of each Dam-KDM5 fusion protein (or Dam alone control) in its respective wild-type or *Kdm5* allele background for three days during early adulthood (3–5 days old). A total of 5,893 binding sites, primarily at promoter regions, were observed across $KDM5^{WT}$, $KDM5^{JmjC*}$, and $KDM5^{L854F}$ (Fig. S4A). Quantification of the differences using NOISeq revealed that $KDM5^{JmjC*}$ and $KDM5^{L854F}$ were associated with more genes showing modest gains than losses in binding (threshold cutoff 0.8; 289 increased vs. 26 decreased in $KDM5^{JmjC*}$ and 216 vs. 20 in $KDM5^{L854F}$, with 120 genes overlapping; Fig. S4B-D; Table S4) [30]. Integrating the TaDa and RNA-seq data did not identify a consistent theme. In both genotypes, of the expressed genes, those that showed increased or decreased TaDa signal were upregulated, downregulated, or unchanged (Fig. S4E, F). Similarly, genes with altered $KDM5^{JmjC*}$ or $KDM5^{L854F}$ TaDa signal showed either unaltered or increased H3K4me3, although many of these genes lacked sufficient H3K4me3 signal to be included in the Diffbind analysis (Fig. S4G, H). Variant KDM5 proteins therefore have slightly increased binding to target genes, but this does not correlate with changes to H3K4me3 or gene expression.

As neither H3K4me3 levels nor KDM5 recruitment explained the transcriptional changes seen in $Kdm5^{JmjC*}$ or $Kdm5^{L854F}$, we examined whether chromatin accessibility might contribute, as KDM5 proteins can interact with nucleosome-positioning chromatin modifiers [19, 55–57]. To do this, we used ATAC-seq to compare the brains of $Kdm5^{JmjC*}$ and $Kdm5^{L854F}$ with those of $Kdm5^{WT}$. Similar to our studies of H3K4me3, KDM5 binding was enriched at regions of open chromatin with the highest ATAC-seq signal (Fig. S5A). Across genotypes, accessible regions were enriched for promoters, and meta-TSS analysis revealed a slight increase in signal at KDM5-bound genes in $Kdm5^{L854F}$ and $Kdm5^{JmjC*}$ (Fig. S5B, C). Quantifying changes in ATAC-seq signal in $Kdm5^{JmjC*}$ brains using Diffbind identified 150 significantly increased and 21 significantly decreased peaks, respectively, that did not correlate with altered expression (Fig. S5D, E; padj < 0.01, log2FC ± 1; Table S5). Likewise, $Kdm5^{L854F}$ had a small number of genes with altered accessibility that did not show concordance with changes to transcription (Fig. S5F, G). Changes in accessibility in $Kdm5^{JmjC*}$ and $Kdm5^{L854F}$ animals are therefore unlikely to be a key contributor to the altered gene expression observed.

Genes commonly downregulated in both $Kdm5^{L854F}$ and $Kdm5^{JmjC*}$ exhibit a characteristic genomic landscape

Our observation that directly regulated target genes in $Kdm5^{JmjC*}$ and $Kdm5^{L854F}$ were remarkably similar,

despite no corresponding change in H3K4me3, KDM5 recruitment, or chromatin accessibility, suggests that other factors influence transcriptional outcomes. One possibility is that pre-existing genomic features of KDM5 target genes play a critical role. Although the variant KDM5^{JmjC*} and KDM5^{L854F} proteins exhibit some unique deficits, the joint activity of the JmjC and C5HC2 domains affected by these variants appears to be essential for regulating a set of 1221 KDM5-bound genes commonly affected in both mutants (common targets; 572 upregulated and 649 downregulated genes; Fig. 2J). To investigate whether baseline chromatin context might contribute to this gene expression program, we examined H3K4me3 and chromatin accessibility at these genes in wild-type brains using existing H3K4me3 CUT&RUN and ATAC-seq data. As expected, based on the strong association between KDM5 binding, H3K4me3, and ATAC-seq, little signal was seen at genes that showed altered gene expression but no KDM5 recruitment (indirect targets; Fig. 4A, B; Fig. S5A; Table S2). However, at direct target genes, we observed that common downregulated target genes exhibited the highest accessibility and H3K4me3 levels, while upregulated genes showed the lowest baseline levels of these chromatin characteristics (Fig. 4C-E). The gene activation program affected by both *Kdm5*^{JmjC*} and *Kdm5*^{L854F} therefore preferentially occurs in this genomic context. Consistent with our knowledge of the shared transcriptional network, genes with high

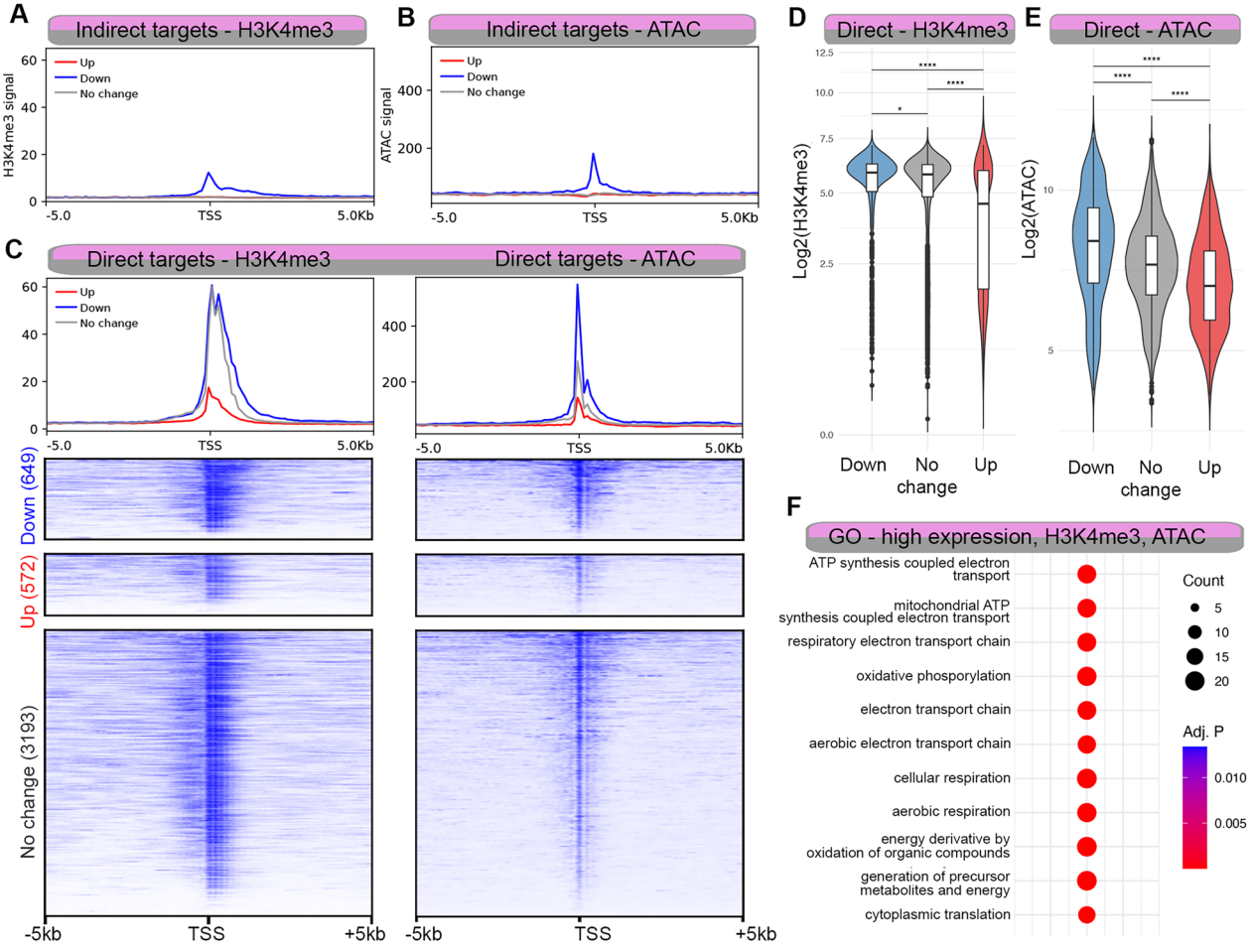

Fig. 4 Promoters of genes downregulated in *Kdm5*^{JmjC*} and *Kdm5*^{L854F} have high H3K4me3 and accessibility. **A** Metaplot showing the distribution of H3K4me3 CUT&RUN (median) signal at genes not bound by KDM5 (indirect targets) relative to the TSS in genes that were upregulated (red), downregulated (blue), or unchanged (gray) in *Kdm5*^{JmjC*} (left) and *Kdm5*^{L854F} (right). Note the same y-axis scale as **C**. **B** Metaplot showing the distribution of ATAC-seq (median) signal at genes not bound by KDM5 (indirect targets) relative to the TSS in genes that were upregulated (red), downregulated (blue), or unchanged (gray) in *Kdm5*^{JmjC*} (left) and *Kdm5*^{L854F} (right). Note the same y-axis scale as **C**. **C** Metaplots and heatmaps of H3K4me3 and ATAC-seq at direct targets separated by upregulated (red), downregulated (blue), and unchanged (gray). **D** Violin plots quantifying promoter H3K4me3 signal (TSS ± 100 bp) at KDM5-bound genes that showed common regulation in *Kdm5*^{JmjC*} and *Kdm5*^{L854F}. * $p < 0.05$, **** $p < 0.0001$ (Kruskal-Wallis test). **E** Violin plots quantifying promoter ATAC signal (TSS ± 100 bp) at KDM5-bound genes that showed common regulation in *Kdm5*^{JmjC*} and *Kdm5*^{L854F}. *** $p < 0.001$ (Kruskal-Wallis test). **F** GO-Biological Process (GO-BP) analyses of KDM5-bound genes in the top 20% of expression (baseMean), H3K4me3, and ATAC-seq of *Kdm5*^{JmjC*} and *Kdm5*^{L854F} commonly regulated genes. Most robustly enriched categories include those related to mitochondrial function and cytoplasmic translation

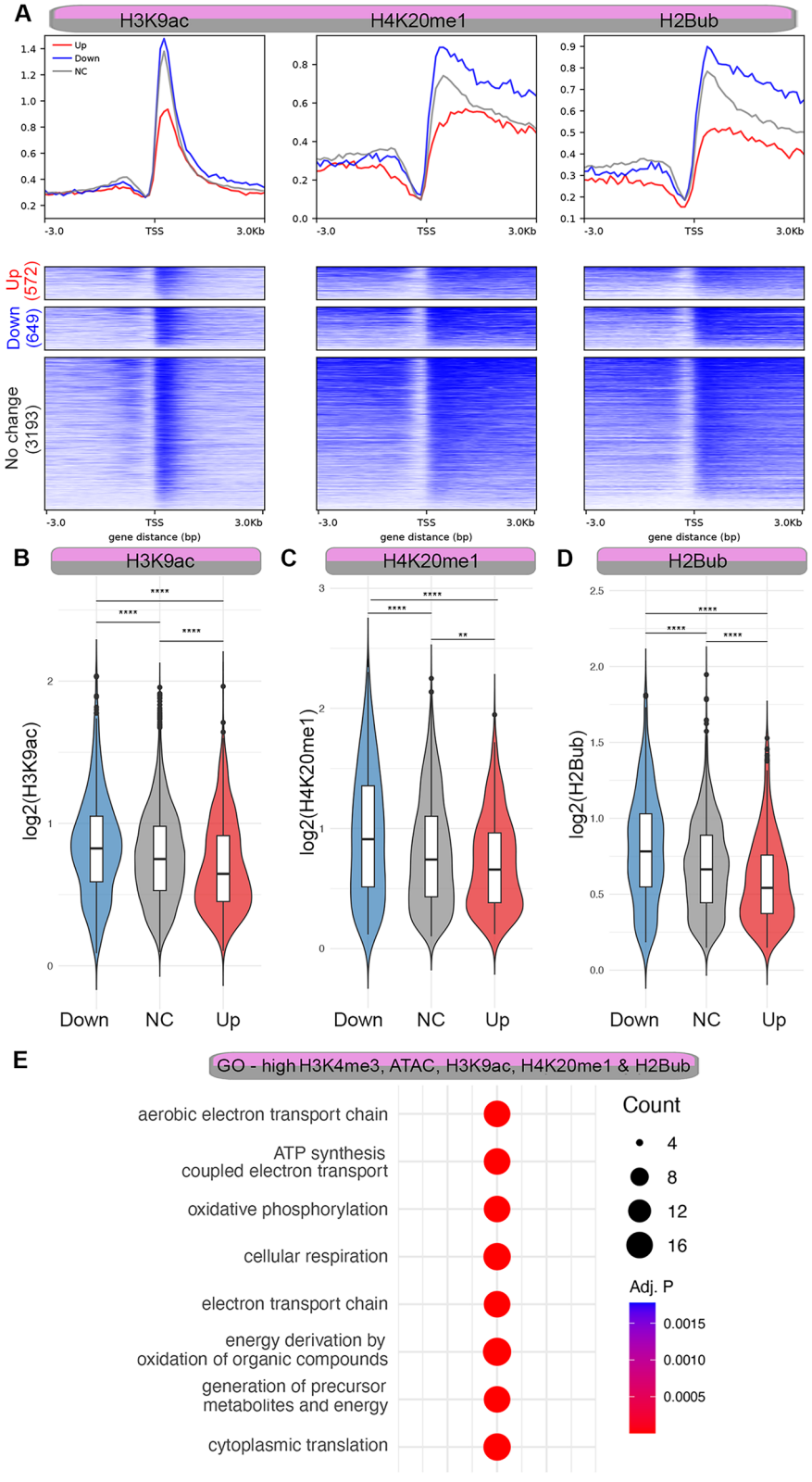

Fig. 5 (See legend on next page.)

(See figure on previous page.)

Fig. 5 Genes downregulated in $Kdm5^{JmjC*}$ and $Kdm5^{L854F}$ correlate with specific promoter and gene body chromatin marks. **A** Metaplots and heatmap using direct common targets showing H3K9ac (adult head ChIP-seq signal), H4K20me1, and H2Bub. Upregulated genes (red), downregulated (blue), or unchanged (gray). **B** Violin plot showing promoter proximal (TSS ± 100 bp) signal from H3K9ac ChIP-seq using KDM5-bound genes that are commonly downregulated ($n = 649$), upregulated (572), or unchanged (NC; 3193). ns = not significant. **** $p < 0.0001$ (Kruskal-Wallis test). **C** Violin plot showing gene body (TSS + 300 to 800 bp) signal from H4K20me1 ChIP-seq using KDM5-bound genes commonly downregulated ($n = 649$), upregulated ($n = 572$), or unchanged (NC; $n = 3193$). **** $p < 0.0001$ ** $p < 0.01$ (Kruskal-Wallis test). **D** Violin plot showing gene body (TSS + 300 to 800 bp) signal from H2Bub ChIP-seq using KDM5-bound genes commonly downregulated ($n = 649$), upregulated ($n = 572$), or unchanged ($n = 3193$; NC). **** $p < 0.0001$ (Kruskal-Wallis test). **E** Gene ontology using genes in the top 30% of signal for ATAC-seq, H3K4me3, H3K9ac, H4K20me1, and H2Bub

H3K4me3 and ATAC-seq signal that were downregulated in $Kdm5^{JmjC*}$ and $Kdm5^{L854F}$ were enriched for categories related to energy metabolism, mitochondrial function, and cytoplasmic translation (top 30% across all categories; Fig. 4F).

To identify additional chromatin modifications that may contribute to KDM5-mediated regulation of transcription of common targets, we used ChIP-Atlas to find histone modification and histone variant datasets generated from adult heads or brains of wild-type animals [44]. These studies revealed that H3K9 acetylation (H3K9ac), H4K20 monomethylation (H4K40me1), and Histone H2B lysine 120 monoubiquitination (H2Bub) showed increased signal at downregulated and/or unchanged genes, and significantly less signal at upregulated genes (Fig. 5A-D; Table S2). The combination of these marks reflects a shared chromatin signature among genes downregulated in both $Kdm5^{JmC*}$ and $Kdm5^{L854F}$, which are enriched for the same GO terms related to translation and mitochondrial function seen previously (Fig. 5E). These data are consistent with prior understanding of the roles of these chromatin marks. For example, H4K20me1 is associated with the expression of "housekeeping" genes, such as those that encode ribosomal and mitochondrial proteins, and H2Bub is needed for efficient deposition of H3K4me3 [58, 59]. In addition to these positive associations, we also observed the converse with the H3K36me3 and the histone variant H2A.V, which co-occur at genes across the genome and showed the lowest signal at downregulated genes (Fig. S6A-E). In contrast to the chromatin signature observed at common targets, genes uniquely regulated in each genotype exhibited distinct behavior (Fig. S7A, B). The most striking feature to emerge from these analyses was the increased accessibility, as assessed by ATAC-seq, observed in genes that were downregulated in $Kdm5^{JmjC*}$ but not in $Kdm5^{L854F}$ (Fig. S7A-C). This is consistent with the JmjC and C5HC2 domains functioning jointly at some target genes, while also exhibiting independent activities. This may also suggest a previously unappreciated role for the JmjC domain in maintaining the expression of genes with highly accessible promoter regions, which were significantly enriched for roles in synaptic signaling (Fig. S7D, E).

Genes repressed by KDM5 via demethylase-dependent mechanisms correlate with chromatin context enriched for H3K36me3 and H2A.V

In addition to investigating links between chromatin features at common KDM5 target genes, we were also interested in those that correlated with potential demethylase-dependent target genes. While the highest levels of the gene body marker H3K36me3 and the promoter-enriched variant histone H2A.V were observed in the commonly unchanged category, a distinct story emerged when examining genes uniquely upregulated in $Kdm5^{JmjC*}$. Whereas genes that were uniquely upregulated in $Kdm5^{L854F}$ showed the lowest levels of H3K36me3 and H2A.V, the 825 genes elevated only in $Kdm5^{JmjC*}$ displayed the highest levels of these chromatin features (Fig. 6A-H; Table S2). Notably, this class of genes does not differ in the extent of H3K4me3 change compared to unchanged genes (Fig. 6I). Indeed, they generally showed smaller changes to H3K4me3 than genes that were upregulated in both genotypes (Common Up compared to Unique Up; Fig. 6I). These data are consistent with demethylase-dependent repression by KDM5 preferentially occurring in a genomic context of high promoter H2A.V and gene body H3K36me3.

Genes upregulated in $Kdm5^{JmjC*}$ with high levels of H3K36me3 and H2A.V were enriched for GO categories connected to neuronal signaling and secretion pathways (Fig. 6J, K).[60] Genes involved in innate immunity were also overrepresented, including components of the Toll and immune deficiency (Imd) pathways. Consistent with this, antimicrobial peptides such as the *Attacin* genes that are activated downstream of these pathways were also elevated uniquely in $Kdm5^{JmjC*}$, although these were not direct targets of KDM5 (Table S1). This is notable in light of emerging links between immunity-related genes and neuronal development and (dys)function [61–63]. Collectively, these data demonstrate that both up- and downregulated genes possess unique combinations of features that are likely to contribute to KDM5-mediated repression and activation (Fig. 7). Furthermore, KDM5-regulated genes within distinct chromatin environments appear to be linked to the regulation of distinct cellular pathways in the brain.

Discussion

Here we explore how KDM5 regulates transcription using the ID-associated allele *Kdm5*^{L854F} and the demethylase-dead *Kdm5*^{JmjC*} strain. While much focus has been on the enzymatic H3K4me3-specific histone demethylase activity of KDM5 proteins, our data further highlight the complexities of these proteins and their roles in gene regulation. *Kdm5*^{L854F} and *Kdm5*^{JmjC*} show both overlapping and unique effects on gene expression that do not correlate with changes in H3K4me3 or promoter accessibility in either genotype. Rather than altered chromatin states, it is the pre-existing chromatin features of genes that seem to influence the outcome of KDM5-regulated transcription. We find that each gene expression category is associated with a specific local chromatin landscape that predicts the gene expression deficits observed in *Kdm5*^{JmjC*} and/or *Kdm5*^{L854F}. These results broaden our understanding of how KDM5 activates or represses transcription in a context-dependent way and point to new pathways as potential contributors to *KDM5* gene-associated ID disorders.

The pathogenic *Kdm5*^{L854F} variant affects the C5HC2 zinc finger motif of KDM5, which appears to be particularly important for gene regulation in the brain, as it is a hotspot for ID-associated variants. At least six other missense variants occur at different residues within this small 51-amino-acid region of KDM5C [1, 64]. The C5HC2 motif is immediately adjacent to the JmjC domain and is considered part of the catalytic cassette [65]. Published in vitro studies of recombinant KDM5C^{L731F}, the human equivalent of KDM5^{L854F}, showed a 50% reduction in activity toward a histone peptide substrate [23]. Our results indicate that in vivo, the enzymatic impairment of KDM5^{L854F} is relatively minor. This may be due to the variant protein having more robust activity within physiologically relevant complexes and/or against nucleosomal substrates, highlighting the importance of analyzing pathogenic variants in a physiological setting. The small number of genes with detectable effects on H3K4me3 in *Kdm5*^{L854F} animals was limited to highly expressed genes, raising the possibility that the catalytic activity of KDM5 is preferentially engaged at promoters of genes with high transcriptional output. In addition to working together for optimal catalytic activity, we propose that the collaboration between the JmjC and C5HC2 domains is also crucial for non-enzymatic mechanisms of transcriptional activation and repression. The KDM5^{JmjC*} and KDM5^{L854F} proteins are largely recruited to their target genes normally, indicating that these changes to KDM5 alter activities downstream of this, such as establishing or stabilizing interactions with other proteins that influence gene expression. Interestingly, the combination of JmjC and C5HC2 domains with non-enzymatic gene regulatory roles may extend beyond KDM5 proteins. For example, JARID2, the founding member of the Jumonji family of proteins, contains both JmjC and C5HC2 motifs, but lacks catalytic residues necessary for histone demethylase activity [66, 67]. These domains therefore also may work in this context to carry out non-enzymatic roles in gene expression regulation.

The transcriptional activation function of KDM5, which is disrupted by *Kdm5*^{L854F} and *Kdm5*^{JmjC*}, is required for the proper expression of genes involved in housekeeping roles, such as those necessary for translation and other critical cellular processes. Given the importance of regulated translation in neurons, we previously proposed that changes in this process may contribute to the cognitive traits observed in patients [9, 11]. Here we show that these genes are generally highly expressed and enriched for a set of promoter and gene body chromatin characteristics known to be associated with transcriptionally active genes [58, 68–70]. While we have observed that *Kdm5*^{JmjC*} and *Kdm5*^{L854F} do not regulate transcription solely through changes to H3K4me3 or accessibility, these features could be critical for KDM5 function. At promoter regions, increased accessibility and elevated levels of H3K4me3 and H3K9ac may promote the recruitment of KDM5. Indeed, across species, KDM5 proteins can interact with histone acetylation regulatory complexes in addition to chromatin remodelers, and a subset of KDM5 proteins can bind to H3K4me3 through their C-terminal PHD motif [18, 46, 55, 71, 72]. Common target genes were also enriched for H2Bub and H4K20me1. H2Bub plays several roles, including promoting H3K4me3 deposition at promoters by allosterically activating the COMPASS methyltransferase complex and facilitating transcriptional elongation [73, 74]. Although not mechanistically linked to H2Bub deposition, H4K20me1 is also found in regions of open chromatin, particularly at housekeeping genes [58, 68]. The combination of these marks likely indicates a permissive chromatin state that promotes productive elongation of RNA polymerase II. Whether or not KDM5 is needed for the efficient deposition or maintenance of H3K9ac, H2Bub, or H4K20me1 will require additional CUT&RUN experiments in *Kdm5*^{JmjC*} and *Kdm5*^{L854F}. In gene contexts where this chromatin signature occurs at low levels, KDM5 appears to repress transcription in a JmjC and C5HC2 domain-dependent manner.

Our results additionally revealed a demethylase-dependent repressive role for KDM5 at a subset of genes marked by elevated levels of promoter H2A.V and genic H3K36me3. How changes to H3K4me3 intersect with the presence of H2A.V and H3K36me3 is not yet clear. *Drosophila* H2A.V combines the functions of two mammalian histone variants, H2A.Z and H2A.X, and has been implicated in both activation and repression of gene expression [75]. Providing a possible link between KDM5

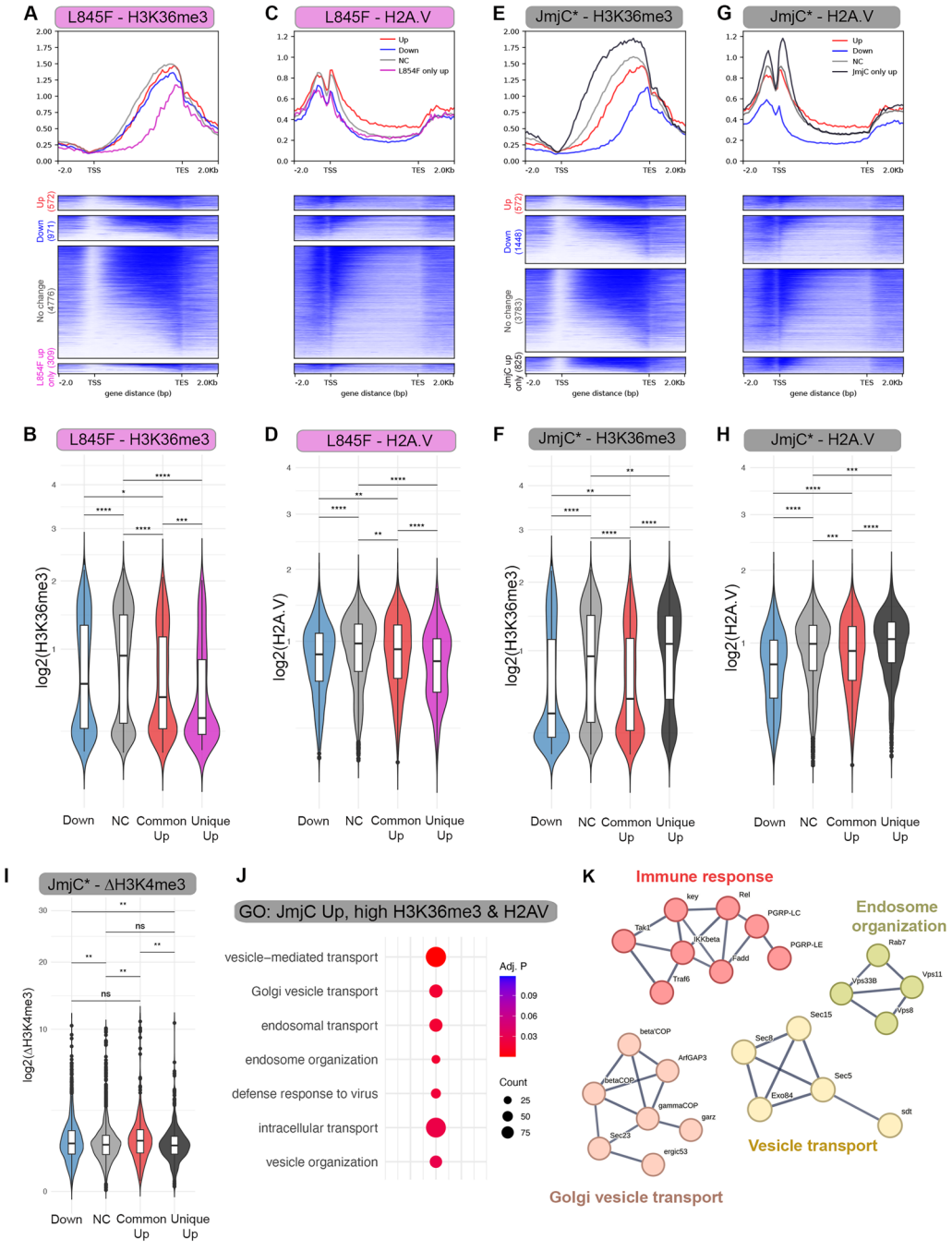

Fig. 6 Genes uniquely upregulated in *Kdm5*^{JmjC*} are enriched for H3K36me3 and H2A.V. **A** Metaplot and heatmap showing H3K36me3 signal adult head ChIP-seq signal relative to the gene body at KDM5-bound genes that were commonly upregulated (red), uniquely upregulated (purple), downregulated (blue), or unchanged (gray) in *Kdm5*^{L854F}. **B** Violin plots quantifying H3K36me3 gene body signal from the categories of genes shown in A. **** $p < 0.0001$, *** $p < 0.001$, * $p < 0.05$ (Kruskal-Wallis test). **C** Metaplot and heatmap showing H2A.V signal adult head ChIP-seq signal relative to the gene body at KDM5-bound genes that were commonly upregulated (red), uniquely upregulated (purple), downregulated (blue), or unchanged (gray) in *Kdm5*^{L854F}. **D** Violin plots quantifying H2A.V promoter-proximal signal from the categories of genes shown in C. **** $p < 0.0001$, *** $p < 0.001$, ** $p < 0.01$ (Kruskal-Wallis test). **E** Metaplot and heatmap showing H3K36me3 signal adult head ChIP-seq signal relative to the gene body at KDM5-bound genes that were commonly upregulated (red), uniquely upregulated (black), downregulated (blue), or unchanged (gray) in *Kdm5*^{JmC*}. **F** Violin plots quantifying H3K36me3 signal from the categories of genes shown in **E**. **** $p < 0.0001$, *** $p < 0.001$, * $p < 0.05$ (Kruskal-Wallis test). **G** Metaplot and heatmap showing H2A.V signal adult head ChIP-seq signal (SRX287772) relative to the gene body at KDM5-bound genes that were commonly upregulated (red), uniquely upregulated (black), downregulated (blue), or unchanged (gray) in *Kdm5*^{Jmjc*}. **H** Violin plots quantifying H2A.V signal from the categories of genes shown in G. **** $p < 0.0001$, *** $p < 0.001$ (Kruskal-Wallis test). **I** Diffbind-generated data showing change to H3K4me3 (ΔH3K4me3) comparing *Kdm5*^{JmjC*} to *Kdm5*^{WT} at genes downregulated (blue; $n = 940$), unchanged (gray; $n = 2150$), commonly upregulated (red; $n = 280$), and uniquely upregulated (black; $n = 506$) in *Kdm5*^{JmjC*}. ** $p < 0.01$, ns = not significant (Kruskal-Wallis test). **J** GO analyses of genes uniquely upregulated in *Kdm5*^{JmjC*} with high (top 30%) of H3K36me3 (gene body) and H2A.V (promoter). **K** String-DataBase-guided examples of genes within categories identified in GO analyses

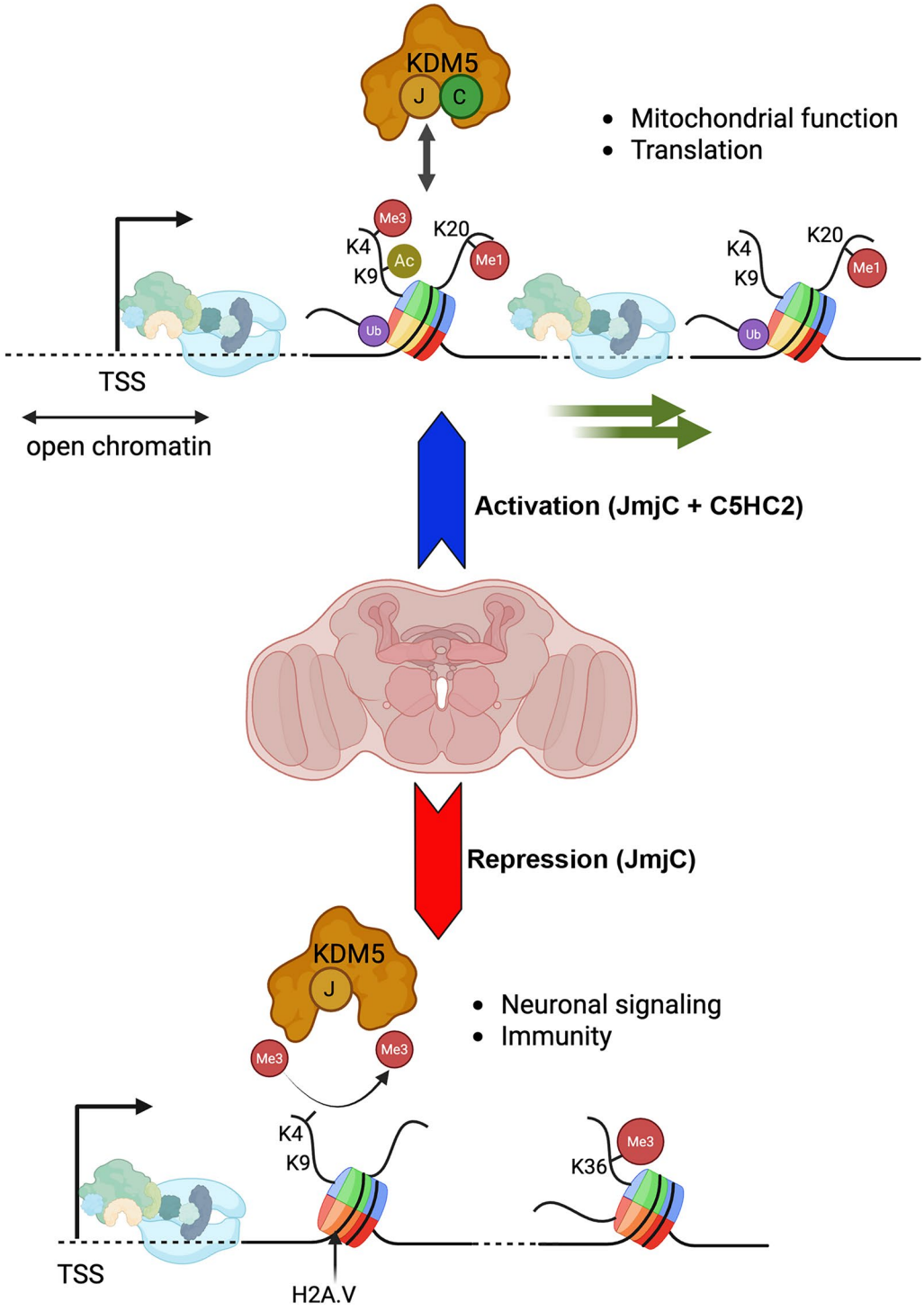

Fig. 7 Model for KDM5 function. Genes that were downregulated in *Kdm5*^{JmjC*} and *Kdm5*^{L854F} exhibited a characteristic signature, characterized by high levels of promoter accessibility, H3K4me3, and H3K9 acetylation. In the gene body, downregulated genes tended to have H4K20me1 and H2Bub. Genes uniquely upregulated in *Kdm5*^{JmjC*} exhibited high H2A.V at the promoter and H3K36me3 in the coding region. Within the KDM5 protein, the orange circle with "J" indicates the JmjC domain, while the green "C" indicates the C5HC2 motif. KDM5-regulated genes in these distinct chromatin environments are involved in different cellular processes. Histone octamer: H3 = blue, H4 = green, H2A = yellow, H2A.V = orange, H2B = red. Images created using BioRender (with permission)

to H2A.V, this histone variant is deposited at promoters by the ATPase Domino (Dom), which we identified as a candidate KDM5 interactor in TurboID studies [55]. Through its interaction with Dom and other members of the SWR1 complex, KDM5 might facilitate H2A.V deposition, or conversely, be recruited to these promoters. Unlike H2A.V, whose localization at promoters overlaps with KDM5 binding, H3K36me3 is deposited within gene bodies during transcription. It is associated with a range of transcriptional activities, including the suppression of spurious transcription, regulation of splicing, and deposition of m6A on mRNAs [76–78]. These H3K36me3-mediated activities are likely to be particularly important in neurons, as genetic disruption to the machinery that regulates this mark is associated with intellectual disability disorders [77]. Similar to H2A.V, although the relationship between KDM5-mediated changes to H3K4me3 and H3K36me3 remains to be determined, it is notable that KDM5 proteins in mammals and *Drosophila* interact with the H3K36me2/3-binding protein MRG15 [55, 56, 71, 79].

KDM5-repressed target genes with high H3K36me3 levels included components of innate immune signaling pathways, such as the Toll and Imd pathways, as well as their downstream antimicrobial peptides. Although traditionally studied in the context of host defense, these immune pathways also have emerging roles in the nervous system, where they influence neuronal survival, synaptic pruning and plasticity, glia-neuron communication, and responses to stress or injury [62, 63, 80]. Together, these findings suggest that KDM5 actively restrains immune gene expression in the brain, potentially to prevent deleterious activation of inflammatory or stress pathways that may compromise neuronal development or function. The loss of KDM5-mediated repression of immune signaling may represent a previously unrecognized mechanism that contributes to the pathogenesis of KDM5-induced ID disorders through neuroimmune dysregulation.

Supplementary Information

The online version contains supplementary material available at https://doi.org/10.1186/s13072-025-00644-z.

Supplementary Material 1.

Supplementary Material 2.

Supplementary Material 3.

Supplementary Material 4.

Supplementary Material 5.

Supplementary Material 6. Supplemental Fig. 1: Predicted changes to the structure of KDM5C. **A** AlphaFold models of Human KDM5^{WT}, KDM5^{JmjC*}, and KDM5^{L854F} proteins. The first column shows full-length proteins with the C%HC2 and JmjC domains circled. The second column shows the JmjC domain in KDM5C^{WT}, KDM5C^{JmjC*} (H514A, E516A), and KDM5C^{L731F} proteins. The side chains altered in the demethylase-dead KDM5C^{JmjC*} protein (positions 514 and 516) are highlighted in red. The third column shows the C5HC2 domain in KDM5C^{WT}, KDM5C^{JmjC*}, and KDM5C^{L731F} proteins. The side chain at 731 is shown in red. **B** Overlay of full-length wild-type ***Drosophila*** KDM5, KDM5^{JmjC*}, and KDM5^{L854F} (gray) compared to human KDM5C (black).

Supplementary Material 7. Supplemental Fig. 2: KDM5 binds to highly expressed genes. **A** Quantification of gene body (TSS + 300–800 bp) signal for RNA polymerase II at KDM5-bound (orange) and unbound (blue) genes. **** $p < 0.0001$ (Kruskal-Wallis test). **B** baseMean values of KDM5-bound (direct; orange) and unbound (indirect; blue) targets that were downregulated, unchanged, or upregulated in ***Kdm5^{JmjC*}*** RNA-seq data. **** $p < 0.0001$ (Kruskal-Wallis test). Gene numbers are provided on the x-axis in all panels. **C** Gene body (TSS + 300–800 bp) signal for RNA polymerase II of KDM5-bound (direct; orange) and unbound (indirect; blue) targets that were downregulated, unchanged, or upregulated in ***Kdm5^{JmjC*}*** RNA-seq data. **** $p < 0.0001$ (Kruskal-Wallis test). **D** baseMean values of KDM5-bound (direct; orange) and unbound (indirect; blue) targets that were downregulated, unchanged, or upregulated in ***Kdm5^{L854F}*** RNA-seq data. **** $p < 0.0001$ (Kruskal-Wallis test). **E** Gene body (TSS + 300–800 bp) signal for RNA polymerase II of KDM5-bound (direct; orange) and unbound (indirect; blue) targets that were downregulated, unchanged, or upregulated in ***Kdm5^{L854F}*** RNA-seq data. **** $p < 0.0001$ (Kruskal-Wallis test).

Supplementary Material 8. Supplemental Fig. 3: Increased H3K4me3 in Kdm5^{JmjC*} does not correlate with elevated gene expression. **A** Pie charts showing the distribution of genomic features within H3K4me3 called peaks (Genrich) for ***Kdm5^{WT}***, ***Kdm5^{JmjC*}***, and ***Kdm5^{L854F}***. **B** Metaplots and heatmaps showing KDM5 and H3K4me3 from ***Kdm5^{WT}***, ***Kdm5^{JmjC*}*** and ***Kdm5^{L854F}*** showing similar genomic distribution. **C** Violin plots showing Diffbind-derived quantification of the change to H3K4me3 signal (log2 of ΔH3K4me3) obtained when examining KDM5-bound (direct) genes in from ***Kdm5^{JmjC*}*** data. Upregulated (red), downregulated (blue), or unchanged (NC; gray). ns = not significant. ** $p < 0.01$ (Kruskal-Wallis test). **D** Violin plots genes with significantly increased H3K4me3 (Diffbind; log2 of ΔH3K4me3) examining KDM5-bound (direct) genes in from ***Kdm5^{JmjC*}*** data. Upregulated (red), downregulated (blue), or unchanged (NC; gray). ns = not significant. ** $p < 0.01$ (Kruskal-Wallis test). Of the 1516 genes with increased H3K4me3, 25 genes were excluded from these analyses because they were expressed at very low levels and not included in our DESeq2 data. **E** MA plot using data from ***Kdm5^{JmjC*}*** RNA-seq, with genes that showed increased H3K4me3 in both ***Kdm5^{JmjC*}*** and ***Kdm5^{L854F}*** highlighted in black. **F** MA plot using data from ***Kdm5^{L854F}*** RNA-seq, with genes that showed increased H3K4me3 in both ***Kdm5^{JmjC*}*** and ***Kdm5^{L854F}*** highlighted in purple. **G** Violin plot showing level of gene body RNA polymerase II signal from genes with increased H3K4me3 in ***Kdm5^{JmjC*}*** and ***Kdm5^{L854F}*** (green, 188 genes) compared to all other expressed genes (orange).

Supplementary Material 9. Supplemental Fig. 4: Binding of KDM5^{JmjC*} and KDM5^{L854F} compared to KDM5^{WT}. **A** Pie charts showing the distribution of wild-type KDM5, KDM5^{JmjC*}, and KDM5^{L854F} TaDa peak annotations. **B** Volcano plot showing the distribution of KDM5^{JmjC*} TaDa data compared to KDM5^{WT} using NOIseq. Genes with significantly more or less signal are indicated by the black dots ($p < 0.2$). **C** Volcano plot showing the distribution of KDM5^{L854F} TaDa data compared to KDM5^{WT} using NOIseq. Genes with significantly more or less signal are indicated by the purple dots ($p < 0.2$). **D** Venn diagrams showing the overlap in significantly altered TaDa signal using KDM5^{JmjC*} and KDM5^{L854F}. **E** Stacked bar graph showing the proportion of genes with increased or decreased KDM5^{JmjC*} TaDa signal that show altered gene expression from RNA-seq data. An additional 2 and 4 genes showed altered TaDa signal consistent with increased or decreased binding, respectively, but lacked corresponding DESeq2 RNA-seq data. **F** Stacked bar graph showing the proportion of genes with increased or decreased KDM5^{L854F} TaDa signal that show altered gene expression from RNA-seq data. **G** Stacked bar graph showing the proportion of genes with increased or decreased KDM5^{JmjC*} TaDa signal (NOIseq) that show altered H3K4me3 (Diffbind). An additional 129 and 6 genes showed altered TaDa signal consistent with increased or decreased binding, respectively, but lacked corresponding Diffbind data. **H** Stacked bar graph showing the proportion of genes with increased or decreased TaDa signal in KDM5^{L854F} TaDa (NOIseq) that show altered H3K4me3 (Diffbind). An additional 61 and 7 genes showed altered TaDa signal consistent with increased or

decreased binding, respectively, but lacked corresponding Diffbind data.

Supplementary Material 10. Supplemental Fig. 5: Altered chromatin accessibility does not correlate with changes to gene expression in ***Kdm5^{JmjC*}*** and ***Kdm5^{L854F}***. **A** Metaplots and heatmaps showing KDM5, H3K4me3 and ATAC-seq from wild-type animals showing similar genomic distribution. **B** Pie chart illustrating the distribution of ATAC-seq called peaks in ***Kdm5^{WT}***, ***Kdm5^{JmjC*}***, and ***Kdm5^{L854F}*** brains according to genomic features based on ChIPseeker annotations. **C** Metaplot showing ATAC-seq signal surrounding the TSS from ***Kdm5^{WT}*** (black), ***Kdm5^{JmjC*}*** (gray), and ***Kdm5^{L854F}*** (purple) adult brains. **D** Volcano plot showing KDM5-bound genes for which the ATAC-seq signal was significantly different comparing ***Kdm5^{JmjC*}*** to ***Kdm5^{WT}***. Black dots indicate a significant difference based on Diffbind data. The number of genes in each category is indicated on the plot (down = 21, up = 150, unchanged = 5362). **E** Stacked bar graph separating genes with increased or decreased ATAC-seq signal and the proportion of genes within these two categories that were upregulated (red), downregulated (blue), or unchanged (gray) in ***Kdm5^{JmjC*}*** RNA-seq data. **F** Volcano plot showing KDM5-bound genes for which ATAC-seq signal was significantly different ***between Kdm5^{L854F}*** and ***Kdm5^{WT}***. Purple dots indicate a significant difference based on Diffbind data. The number of genes in each category is indicated on the plot (down = 19, up = 35, unchanged = 5479). **G** Stacked bar graph separating genes with increased or decreased ATAC-seq signal and the proportion of genes within these two categories that were upregulated (red), downregulated (blue), or unchanged (gray) in ***Kdm5^{L854F}*** RNA-seq data.

Supplementary Material 11. Supplemental Fig. 6: association between chromatin marks and altered gene expression in Kdm5^{JmjC*} and Kdm5^{L854F}. **A** Meta plot and heatmap showing H3K36me3 signal at common upregulated (red), downregulated (blue), or unchanged (gray) genes. **B** Violin plots quantifying changes to H3K36 in the gene body (TSS + 300 to + 800 bp) at upregulated (red), downregulated (blue), or unchanged (gray) genes. ns = not significant. ** $p < 0.001$, **** $p < 0.0001$ (Kruskal-Wallis test). **C** Meta plot and heatmap showing H2A.V signal at common upregulated (red), downregulated (blue), or unchanged (gray) genes. **D** Violin plots quantifying changes to H2A.V at promoter regions at upregulated (red), downregulated (blue), or unchanged (gray) genes. **** $p < 0.0001$ (Kruskal-Wallis test). **E** Meta plots and heatmaps showing that genes with high promoter H2A.V are likely to also have high H3K36me3 in the gene body.

Supplementary Material 12. Supplemental Fig. 7: Association between chromatin marks and altered gene expression unique to ***Kdm5^{JmjC*}*** or ***Kdm5^{L854F}***. **A** Meta plot and heatmap showing H3K4me3, ATAC-seq (both relative to the TSS), H3K9ac, H2Bub and H4K20me (TSS to TES) signal at ***Kdm5^{JmjC*}*** uniquely upregulated (red), downregulated (blue), or unchanged (gray) genes. **B** Meta plot and heatmap showing H3K4me3, ATAC-seq (both relative to the TSS), H3K9ac, H2Bub and H4K20me (TSS to TES) signal at ***Kdm5^{L854F}*** uniquely upregulated (red), downregulated (blue), or unchanged (gray) genes. **C** Violin plot quantifying changes to ATAC signal (Diffbind) at upregulated (red), downregulated (blue), or unchanged (gray) genes in ***Kdm5^{JmjC*}***. *** $p < 0.001$, **** $p < 0.0001$ (Kruskal-Wallis test). n = gene numbers in each category. **D** GO of uniquely downregulated genes in ***Kdm5^{JmjC*}***. **E** GO and String-db-guided genes within the synaptic signaling category.

Acknowledgements
We thank Hayden A.M. Hatch for producing the ID-variant Targeted DamID fly stocks and Owen Marshall for invaluable discussions about TaDa analyses. We are grateful to Aubrey Siebels, Bethany Terry, Richard D. Kelly IV, Hill Gregoire, Amira Mahoney, and other members of the Secombe lab, the Einstein chromatin club, and the Einstein Intellectual and Developmental Disabilities Research Center (IDDRC) for their support and feedback throughout this project. We appreciate the availability of fly strains from the Bloomington Drosophila Stock Center (NIH P400D018537). At Albert Einstein College of Medicine, we thank the Genomics core facilities and the Einstein Cancer Center Support Grant (P30 CA013330).

Author contributions
Conceptualization, MY, JS; Methodology, MY, MC, JS; Investigation, MY, MC, JS; Writing – original draft, MY, JS; Writing – reviewing and editing, MY, MC, JS; Funding acquisition, JS, MY, MC; Supervision, JS.

Funding
National Institutes of Health grant T32GM149364 (MY). National Institutes of Health grant F31GM146347 (MY). National Institutes of Health grant R01GM1112783 (JS). National Institutes of Health grant R01GM150189 (JS). National Institutes of Health grant F31GM150194 (MC). National Institutes of Health grant T32GM145438 (MC).
Irma T. Hirschl Trust (JS).

Data availability
All fly strains used in this study are available upon request. New genomic data generated as part of this study are available under BioProject reference: PRJNA1188621 and GEO as follows: H3K4me3 CUT&RUN (GSE282535), Targeted DamID (GSE282537), ATAC-Seq (GSE282534).

Declarations

Ethics approval and consent to participate
Not applicable.

Consent for publication
Not applicable.

Competing interests
The authors declare no competing interests.

Received: 16 July 2025 / Accepted: 1 November 2025
Published online: 03 December 2025

References

1. Hatch HAM, Secombe J. Molecular and cellular events linking variants in the histone demethylase KDM5C to the intellectual disability disorder Claes-Jensen syndrome. FEBS J. 2022;289:7776–87. https://doi.org/10.1111/febs.16204.
2. Iwase S, Bérubé NG, Zhou Z, Kasri NN, Battaglioli E, Scandaglia M, Barco A. Epigenetic etiology of intellectual disability. J Neurosci. 2017;37:10773–82. https://doi.org/10.1523/JNEUROSCI.1840-17.2017.
3. Vallianatos CN, Iwase S. Disrupted intricacy of histone H3K4 methylation in neurodevelopmental disorders. Epigenomics. 2015;7:503–19. https://doi.org/10.2217/epi.15.1.
4. Faundes V, Newman WG, Bernardini L, Canham N, Clayton-Smith J, Dallapiccola B, Davies SJ, Demos MK, Goldman A, Gill H, et al. Histone lysine Methylases and demethylases in the landscape of human developmental disorders. Am J Hum Genet. 2018;102:175–87. https://doi.org/10.1016/j.ajhg.2017.11.013.
5. Pérez-Sisqués L, Bhatt SU, Matuleviciute R, Gileadi TE, Kramar E, Graham A, Garcia FG, Keiser A, Matheos DP, Cain JA, et al. The intellectual disability risk gene Kdm5b regulates Long-Term memory consolidation in the hippocampus. J Neurosci. 2024;44. https://doi.org/10.1523/JNEUROSCI.1544-23.2024.
6. Iwase S, Brookes E, Agarwal S, Badeaux AI, Ito H, Vallianatos CN, Tomassy GS, Kasza T, Lin G, Thompson A, et al. A mouse model of X-linked intellectual disability associated with impaired removal of histone methylation. Cell Rep. 2016;14:1000–9. https://doi.org/10.1016/j.celrep.2015.12.091.
7. Vallianatos CN, Farrehi C, Friez MJ, Burmeister M, Keegan CE, Iwase S. Altered Gene-Regulatory function of KDM5C by a novel mutation associated with autism and intellectual disability. Front Mol Neurosci. 2018;11:104. https://doi.org/10.3389/fnmol.2018.00104.
8. El Hayek L, Tuncay IO, Nijem N, Russell J, Ludwig S, Kaur K, Li X, Anderton P, Tang M, Gerard A et al. (2020). KDM5A mutations identified in autism spectrum disorder using forward genetics. eLife *9*. https://doi.org/10.7554/eLife.56883
9. Yheskel M, Hatch HAM, Pedrosa E, Terry BK, Siebels AA, Zheng XY, Blok LER, Fencková M, Sidoli S, Schenck A, et al. KDM5-mediated transcriptional activation of ribosomal protein genes alters translation efficiency to regulate mitochondrial metabolism in neurons. Nucleic Acids Res. 2024;52:6201–19. https://doi.org/10.1093/nar/gkae261.
10. Belalcazar HM, Hendricks EL, Zamurrad S, Liebl FLW, Secombe J. The histone demethylase KDM5 is required for synaptic structure and function at the drosophila neuromuscular junction. Cell Rep. 2021;34:108753. https://doi.org/10.1016/j.celrep.2021.108753.

11. Zamurrad S, Hatch HAM, Drelon C, Belalcazar HM, Secombe J. A drosophila model of intellectual disability caused by mutations in the histone demethylase KDM5. Cell Rep. 2018;22:2359–69. https://doi.org/10.1016/j.celrep.2018.02.018.
12. Hatch HAM, O'Neil MH, Marion RW, Secombe J, Shulman LH. Caregiver-reported characteristics of children diagnosed with pathogenic variants in KDM5C. Am. J Med Genet A. 2021;185:2951–8. https://doi.org/10.1002/ajmg.a.62381.
13. Wu P-M, Yu W-H, Chiang C-W, Wu C-Y, Chen J-S, Tu Y-F. Novel variations in the KDM5C gene causing X-Linked intellectual disability. Neurol Genet. 2022;8:e646. https://doi.org/10.1212/NXG.0000000000000646.
14. Benayoun BA, Pollina EA, Ucar D, Mahmoudi S, Karra K, Wong ED, Devarajan K, Daugherty AC, Kundaje AB, Mancini E, et al. H3K4me3 breadth is linked to cell identity and transcriptional consistency. Cell. 2014;158:673–88. https://doi.org/10.1016/j.cell.2014.06.027.
15. Wang H, Fan Z, Shliaha PV, Miele M, Hendrickson RC, Jiang X, Helin K. H3K4me3 regulates RNA polymerase II promoter-proximal pause-release. Nature. 2023;615:339–48. https://doi.org/10.1038/s41586-023-05780-8.
16. Beacon TH, Delcuve GP, López C, Nardocci G, Kovalchuk I, van Wijnen AJ, Davie JR. The dynamic broad epigenetic (H3K4me3, H3K27ac) domain as a mark of essential genes. Clin Epigenetics. 2021;13:138. https://doi.org/10.1186/s13148-021-01126-1.
17. Vallianatos CN, Raines B, Porter RS, Bonefas KM, Wu MC, Garay PM, Collette KM, Seo YA, Dou Y, Keegan CE, et al. Mutually suppressive roles of KMT2A and KDM5C in behaviour, neuronal structure, and histone H3K4 methylation. Commun Biol. 2020;3:278. https://doi.org/10.1038/s42003-020-1001-6.
18. Ohguchi Y, Ohguchi H. Diverse functions of KDM5 in cancer: transcriptional repressor or activator? Cancers (Basel). 2022;14. https://doi.org/10.3390/cancers14133270.
19. Kurup JT, Campeanu IJ, Kidder BL. Contribution of H3K4 demethylase KDM5B to nucleosome organization in embryonic stem cells revealed by micrococcal nuclease sequencing. Epigenetics Chromatin. 2019;12:20. https://doi.org/10.1186/s13072-019-0266-9.
20. Zhang S-M, Cai WL, Liu X, Thakral D, Luo J, Chan LH, McGeary MK, Song E, Blenman KRM, Micevic G, et al. KDM5B promotes immune evasion by recruiting SETDB1 to silence retroelements. Nature. 2021;598:682–7. https://doi.org/10.1038/s41586-021-03994-2.
21. Jensen LR, Amende M, Gurok U, Moser B, Gimmel V, Tzschach A, Janecke AR, Tariverdian G, Chelly J, Fryns J-P, et al. Mutations in the JARID1C gene, which is involved in transcriptional regulation and chromatin remodeling, cause X-linked mental retardation. Am J Hum Genet. 2005;76:227–36. https://doi.org/10.1086/427563.
22. Claes S, Devriendt K, Van Goethem G, Roelen L, Meireleire J, Raeymaekers P, Cassiman JJ, Fryns JP. Novel syndromic form of X-linked complicated spastic paraplegia. Am J Med Genet. 2000;94:1–4.
23. Iwase S, Lan F, Bayliss P, de la Torre-Ubieta L, Huarte M, Qi HH, Whetstine JR, Bonni A, Roberts TM, Shi Y. The X-linked mental retardation gene SMCX/JARID1C defines a family of histone H3 lysine 4 demethylases. Cell. 2007;128:1077–88. https://doi.org/10.1016/j.cell.2007.02.017.
24. Drelon C, Rogers MF, Belalcazar HM, Secombe J. The histone demethylase KDM5 controls developmental timing in drosophila by promoting prothoracic gland endocycles. Development. 2019;146. https://doi.org/10.1242/dev.182568.
25. Rogers MF, Marshall OJ, Secombe J. KDM5-mediated activation of genes required for mitochondrial biology is necessary for viability in drosophila. Development. 2023;150. https://doi.org/10.1242/dev.202024.
26. Abramson J, Adler J, Dunger J, Evans R, Green T, Pritzel A, Ronneberger O, Willmore L, Ballard AJ, Bambrick J, et al. Accurate structure prediction of biomolecular interactions with alphafold 3. Nature. 2024;630:493–500. https://doi.org/10.1038/s41586-024-07487-w.
27. Michaud-Agrawal N, Denning EJ, Woolf TB, Beckstein O. MDAnalysis: a toolkit for the analysis of molecular dynamics simulations. J Comput Chem. 2011;32:2319–27. https://doi.org/10.1002/jcc.21787.
28. Marshall OJ, Brand AH. damidseq_pipeline: an automated pipeline for processing DamID sequencing datasets. Bioinformatics. 2015;31:3371–3. https://doi.org/10.1093/bioinformatics/btv386.
29. Yu G, Wang L-G, He Q-Y. ChIPseeker: an R/Bioconductor package for chip peak annotation, comparison and visualization. Bioinformatics. 2015;31:2382–3. https://doi.org/10.1093/bioinformatics/btv145.
30. Tarazona S, Furió-Tarí P, Turrà D, Pietro AD, Nueda MJ, Ferrer A, Conesa A. Data quality aware analysis of differential expression in RNA-seq with NOISeq R/Bioc package. Nucleic Acids Res. 2015;43:e140. https://doi.org/10.1093/nar/gkv711.
31. Xu C, Ramos TB, Rogers EM, Reiser MB, Doe CQ. (2024). Homeodomain proteins hierarchically specify neuronal diversity and synaptic connectivity. eLife *12*. https://doi.org/10.7554/eLife.90133
32. Chen S, Zhou Y, Chen Y, Gu J. Fastp: an ultra-fast all-in-one FASTQ preprocessor. Bioinformatics. 2018;34:i884–90. https://doi.org/10.1093/bioinformatics/bty560.
33. Liao Y, Smyth GK, Shi W. The R package Rsubread is easier, faster, cheaper and better for alignment and quantification of RNA sequencing reads. Nucleic Acids Res. 2019;47:e47. https://doi.org/10.1093/nar/gkz114.
34. Li H, Handsaker B, Wysoker A, Fennell T, Ruan J, Homer N, Marth G, Abecasis G, Durbin R. The Sequence Alignment/Map format and SAMtools. Bioinformatics. 2009;25:2078–9. https://doi.org/10.1093/bioinformatics/btp352. and 1000 Genome Project Data Processing Subgroup.
35. Ramírez F, Dündar F, Diehl S, Grüning BA, Manke T. DeepTools: a flexible platform for exploring deep-sequencing data. Nucleic Acids Res. 2014;42:W187–91. https://doi.org/10.1093/nar/gku365.
36. Genrich GJ. Detecting Sites of Genomic Enrichment. https://github.com/jsh58/Genrich
37. Ross-Innes CS, Stark R, Teschendorff AE, Holmes KA, Ali HR, Dunning MJ, Brown GD, Gojis O, Ellis IO, Green AR, et al. Differential oestrogen receptor binding is associated with clinical outcome in breast cancer. Nature. 2012;481:389–93. https://doi.org/10.1038/nature10730.
38. Yu G, Wang L-G, Han Y, He Q-Y. ClusterProfiler: an R package for comparing biological themes among gene clusters. OMICS. 2012;16:284–7. https://doi.org/10.1089/omi.2011.0118.
39. Ramírez F, Bhardwaj V, Arrigoni L, Lam KC, Grüning BA, Villaveces J, Habermann B, Akhtar A, Manke T. High-resolution tads reveal DNA sequences underlying genome organization in flies. Nat Commun. 2018;9:189. https://doi.org/10.1038/s41467-017-02525-w.
40. Lopez-Delisle L, Rabbani L, Wolff J, Bhardwaj V, Backofen R, Grüning B, Ramírez F, Manke T. PyGenomeTracks: reproducible plots for multivariate genomic datasets. Bioinformatics. 2021;37:422–3. https://doi.org/10.1093/bioinformatics/btaa692.
41. Wickham H. ggplot2: elegant graphics for data analysis (Use R!). 2nd ed. Springer; 2016.
42. Liu X, Secombe J. The histone demethylase KDM5 activates gene expression by recognizing chromatin context through its PHD reader motif. Cell Rep. 2015;13:2219–31. https://doi.org/10.1016/j.celrep.2015.11.007.
43. Kharchenko PV, Alekseyenko AA, Schwartz YB, Minoda A, Riddle NC, Ernst J, Sabo PJ, Larschan E, Gorchakov AA, Gu T, et al. Comprehensive analysis of the chromatin landscape in drosophila melanogaster. Nature. 2011;471:480–5. https://doi.org/10.1038/nature09725.
44. Oki S, Ohta T, Shioi G, Hatanaka H, Ogasawara O, Okuda Y, Kawaji H, Nakaki R, Sese J, Meno C. ChIP-Atlas: a data-mining suite powered by full integration of public ChIP-seq data. EMBO Rep. 2018;19. https://doi.org/10.15252/embr.201846255.
45. Secombe J, Li L, Carlos L, Eisenman RN. The trithorax group protein lid is a trimethyl histone H3K4 demethylase required for dMyc-induced cell growth. Genes Dev. 2007;21:537–51. https://doi.org/10.1101/gad.1523007.
46. Pavlenko E, Ruengeler T, Engel P, Poepsel S. Functions and interactions of mammalian KDM5 demethylases. Front Genet. 2022;13:906662. https://doi.org/10.3389/fgene.2022.906662.
47. Washington NL, Stinson EO, Perry MD, Ruzanov P, Contrino S, Smith R, Zha Z, Lyne R, Carr A, Lloyd P et al. (2011). The modENCODE Data Coordination Center: lessons in harvesting comprehensive experimental details. Database (Oxford) *2011*, bar023. https://doi.org/10.1093/database/bar023
48. Hainer SJ, Fazzio TG. High-Resolution chromatin profiling using CUT&RUN. Curr Protoc Mol Biol. 2019;126:e85. https://doi.org/10.1002/cpmb.85.
49. Meers MP, Bryson TD, Henikoff JG, Henikoff S. (2019). Improved CUT&RUN chromatin profiling tools. eLife *8*. https://doi.org/10.7554/eLife.46314
50. Karwacki-Neisius V, Jang A, Cukuroglu E, Tai A, Jiao A, Predes D, Yoon J, Brookes E, Chen J, Iberg A, et al. WNT signalling control by KDM5C during development affects cognition. Nature. 2024;627:594–603. https://doi.org/10.1038/s41586-024-07067-y.
51. Stark R, Brown GD. DiffBind:differential binding analysis of ChIP-seq peak data. http://bioconductor.org/packages/release/bioc/html/DiffBind.html
52. Marshall OJ, Southall TD, Cheetham SW, Brand AH. Cell-type-specific profiling of protein-DNA interactions without cell isolation using targeted DamID with next-generation sequencing. Nat Protoc. 2016;11:1586–98. https://doi.org/10.1038/nprot.2016.084.

53. Southall TD, Gold KS, Egger B, Davidson CM, Caygill EE, Marshall OJ, Brand AH. Cell-type-specific profiling of gene expression and chromatin binding without cell isolation: assaying RNA pol II occupancy in neural stem cells. Dev Cell. 2013;26:101–12. https://doi.org/10.1016/j.devcel.2013.05.020.
54. Hatch HA, Belalcazar HM, Marshall OJ, Secombe J. A KDM5-Prospero transcriptional axis functions during early neurodevelopment to regulate mushroom body formation. eLife. 2021;10. https://doi.org/10.7554/eLife.63886.
55. Yheskel M, Sidoli S, Secombe J. Proximity labeling reveals a new in vivo network of interactors for the histone demethylase KDM5. Epigenetics Chromatin. 2023;16:8. https://doi.org/10.1186/s13072-023-00481-y.
56. Nishibuchi G, Shibata Y, Hayakawa T, Hayakawa N, Ohtani Y, Sinmyozu K, Tagami H, Nakayama J. Physical and functional interactions between the histone H3K4 demethylase KDM5A and the nucleosome remodeling and deacetylase (NuRD) complex. J Biol Chem. 2014;289:28956–70. https://doi.org/10.1074/jbc.M114.573725.
57. Gong F, Clouaire T, Aguirrebengoa M, Legube G, Miller KM. Histone demethylase KDM5A regulates the ZMYND8-NuRD chromatin remodeler to promote DNA repair. J Cell Biol. 2017;216:1959–74. https://doi.org/10.1083/jcb.201611135.
58. Shoaib M, Chen Q, Shi X, Nair N, Prasanna C, Yang R, Walter D, Frederiksen KS, Einarsson H, Svensson JP, et al. Histone H4 lysine 20 mono-methylation directly facilitates chromatin openness and promotes transcription of housekeeping genes. Nat Commun. 2021;12:4800. https://doi.org/10.1038/s41467-021-25051-2.
59. Soares LM, Buratowski S. Histone crosstalk: h2bub and H3K4 methylation. Mol Cell. 2013;49:1019–20. https://doi.org/10.1016/j.molcel.2013.03.012.
60. Szklarczyk D, Gable AL, Lyon D, Junge A, Wyder S, Huerta-Cepas J, Simonovic M, Doncheva NT, Morris JH, Bork P, et al. STRING v11: protein-protein association networks with increased coverage, supporting functional discovery in genome-wide experimental datasets. Nucleic Acids Res. 2019;47:D607–13. https://doi.org/10.1093/nar/gky1131.
61. Lye SH, Chtarbanova S. Drosophila as a model to study brain innate immunity in health and disease. Int J Mol Sci. 2018;19. https://doi.org/10.3390/ijms19123922.
62. Lee S, Silverman N, Gao F-B. Emerging roles of antimicrobial peptides in innate immunity, neuronal function, and neurodegeneration. Trends Neurosci. 2024;47:949–61. https://doi.org/10.1016/j.tins.2024.09.001.
63. Stuart BAR, Franitza AL, E L. Regulatory roles of antimicrobial peptides in the nervous system: implications for neuronal aging. Front Cell Neurosci. 2022;16:843790. https://doi.org/10.3389/fncel.2022.843790.
64. Ghasemi M-R, Esmaeilizadeh Z, Tehrani Fateh S, Sadeghi H, Bagheri S, Hashemi-Gorji F, Sheikhi Nooshabadi M, Madannezhad R, Ghavami T, Mirfakhraie TS, R., et al. Clinical features and genetic characteristics of XLID patients with KDM5C gene mutations: insights on Phenotype-Genotype correlations from 175 previous cases and identification of a novel variant. Mol Genet Genomic Med. 2025;13:e70057. https://doi.org/10.1002/mgg3.70057.
65. Kataria A, Tyagi S. Domain architecture and protein-protein interactions regulate KDM5A recruitment to the chromatin. Epigenetics. 2023;18:2268813. https://doi.org/10.1080/15592294.2023.2268813.
66. Li G, Margueron R, Ku M, Chambon P, Bernstein BE, Reinberg D. Jarid2 and PRC2, partners in regulating gene expression. Genes Dev. 2010;24:368–80. https://doi.org/10.1101/gad.1886410.
67. Sreeshma B, Devi A. JARID2 and EZH2, the eminent epigenetic drivers in human cancer. Gene. 2023;879:147584. https://doi.org/10.1016/j.gene.2023.147584.
68. Crain AT, Butler MB, Hill CA, Huynh M, McGinty RK, Duronio RJ. Drosophila melanogaster Set8 and L(3)mbt function in gene expression independently of histone H4 lysine 20 methylation. Genes Dev. 2024;38:455–72. https://doi.org/10.1101/gad.351698.124.
69. Huynh MT, Sengupta B, Krajewski WA, Lee T-H. Effects of histone H2B ubiquitylations and h3k79me3 on transcription elongation. ACS Chem Biol. 2023;18:537–48. https://doi.org/10.1021/acschembio.2c00887.
70. Talbert PB, Henikoff S. The Yin and Yang of histone marks in transcription. Annu Rev Genomics Hum Genet. 2021;22:147–70. https://doi.org/10.1146/annurev-genom-120220-085159.
71. Lee N, Erdjument-Bromage H, Tempst P, Jones RS, Zhang Y. The H3K4 demethylase lid associates with and inhibits histone deacetylase Rpd3. Mol Cell Biol. 2009;29:1401–10. https://doi.org/10.1128/MCB.01643-08.
72. DiTacchio L, Le HD, Vollmers C, Hatori M, Witcher M, Secombe J, Panda S. Histone lysine demethylase JARID1a activates CLOCK-BMAL1 and influences the circadian clock. Science. 2011;333:1881–5. https://doi.org/10.1126/science.1206022.
73. Chandrasekharan MB, Huang F, Sun Z-W. Histone H2B ubiquitination and beyond: regulation of nucleosome stability, chromatin dynamics and the trans-histone H3 methylation. Epigenetics. 2010;5:460–8. https://doi.org/10.4161/epi.5.6.12314.
74. Mandal K, Tomar SK, Kumar Santra M. Decoding the ubiquitin language: orchestrating transcription initiation and gene expression through chromatin remodelers and histones. Gene. 2024;904:148218. https://doi.org/10.1016/j.gene.2024.148218.
75. Baldi S, Becker PB. The variant histone H2A.V of Drosophila–three roles, two guises. Chromosoma. 2013;122:245–58. https://doi.org/10.1007/s00412-013-0409-x.
76. Sharda A, Humphrey TC. The role of histone H3K36me3 writers, readers and erasers in maintaining genome stability. DNA Repair (Amst). 2022;119:103407. https://doi.org/10.1016/j.dnarep.2022.103407.
77. Zaghi M, Broccoli V, Sessa A. H3K36 methylation in neural development and associated diseases. Front Genet. 2019;10:1291. https://doi.org/10.3389/fgene.2019.01291.
78. Huang H, Weng H, Zhou K, Wu T, Zhao BS, Sun M, Chen Z, Deng X, Xiao G, Auer F, et al. Histone H3 trimethylation at lysine 36 guides m6A RNA modification co-transcriptionally. Nature. 2019;567:414–9. https://doi.org/10.1038/s41586-019-1016-7.
79. Hayakawa T, Ohtani Y, Hayakawa N, Shinmyozu K, Saito M, Ishikawa F, Nakayama J. RBP2 is an MRG15 complex component and down-regulates intragenic histone H3 lysine 4 methylation. Genes Cells. 2007;12:811–26. https://doi.org/10.1111/j.1365-2443.2007.01089.x.
80. Sun J, Rojo-Cortes F, Ulian-Benitez S, Forero MG, Li G, Singh DND, Wang X, Cachero S, Moreira M, Kavanagh D et al. (2024). A neurotrophin functioning with a Toll regulates structural plasticity in a dopaminergic circuit. eLife *13*. https://doi.org/10.7554/eLife.102222

Publisher's note